Summer 2017

# Hydrogeochemical controls on reactive and nonreactive solute transport in heterogenous porous media

Mahta Gholizadeh Ansari



Department:

# HYDROGEOCHEMICAL CONTROLS ON REACTIVE AND NON-REACTIVE SOLUTE TRANSPORT IN HETEROGENOUS POROUS MEDIA

by

MAHTA GHOLIZADEH ANSARI

A THESIS

Presented to the Faculty of the Graduate School of the

MISSOURI UNIVERSITY OF SCIENCE AND TECHNOLOGY

In Partial Fulfillment of the Requirements for the Degree

MASTER OF SCIENCE IN GEOLOGICAL ENGINEERING

2017

Approved by

Dr. Peyman Heidari, Advisor
Dr. Katherine Grote, Co Advisor
Dr. J. David Rogers

## PUBLICATION THESIS OPTION

This thesis consists of the following two articles that have been submitted for publication as follows:

Paper I: Pages 3-44 have been submitted to Geochemical et Cosmochimica acta.

Paper II: Pages 45-75 are intended for submission to Water resource research journal.

# ABSTRACT

This work examines how physical and chemical heterogeneity can affect reactive and non-reactive transport in porous media. The effect of heterogeneity of the porous media is investigated both on dissolution rate of magnesite and attenuation time of non-reactive contaminants in non-reactive media. Various spatial distribution were created using statistical parameters in PETREL.A total of 6793 transport modeling simulations were run using CrunchFlow. Lasso regression was used to select most significant features and those features are then used in linear regression and deep learning models.

The magnesite dissolution simulations were performed under different permeability ratios (magnesite /sand permeability) and inlet pH. The variables used for building different realizations of porous media are mineral abundance, major direction anisotropy and minor direction anisotropy. Overall, permeability ratio had the most significant impact on dissolution rate. Deep learning captured 89.0 % of the variance in the data while linear regression only captured 73.2%.

The bromide transport simulations were conducted under various flow rates and transverse dispersivity values. Different spatial distributions were created with different permeability standard deviations and major and minor direction anisotropies. Standard deviation proved to have the most significant impact on attenuation time, followed by major and minor direction anisotropies A more heterogeneous and anisotropic distribution resulted in a slower concentration reduction. The effect of anisotropies were trivial in a relatively homogenous distributions. The linear model can describe 70.83 % of the variance in the data.

# ACKNOWLEDGMENTS

I would like to express my sincere gratitude to my advisor, Dr. Peyman Heidari, for his guidance, patience, and support. It has been an honor to be his student. I would also like to thank my committee members Dr. Katherine Grote and Dr. J. David Rogers.

I would also like to send my appreciation to my parents, my brother and Nick Anthony for all their support and encouragement throughout my journey as a graduate student.

# TABLE OF CONTENTS

Page

PUBLICATION THESIS OPTION ..... iii

ABSTRACT ..... iv

ACKNOWLEDGMENTS ..... v

LIST OF FIGURES ..... ix

LIST OF TABLES ..... xi

SECTION

1. INTRODUCTION ..... 1

1.1. MINERAL DISSOLUTION ..... 1

1.2. ATTENUATION TIME OF A NON-REACTIVE CONTAMINANT 2

PAPER

I. PREDICTION OF MAGNESITE DISSOLUTION RATE IN HETEOGENOUS POROUS MEDIA USING DEEP LEARNING ..... 3

ABSTRACT ..... 3

1. INTRODUCTION ..... 4

2. METHODOLOGY ..... 8

2.1. MAGNESITE DISSOLUTION ..... 8

2.2. POROUS MEDIA DISCRIPTION ..... 9

2.3. REACTIVE TRANSPORT MODELING ..... 11

2.4. MACHINE LEARNING ..... 14

2.4.1. Feature Selection. ..... 14

2.4.2. Deep Learning ..... 15

3. RESULTS ..... 17

3.1. MAGNESITE ABUNDANCE ..... 17

3.2. PERMEABILITY RATIO ..... 21

3.3. MAJOR DIRECTION ANISOTROPY ..... 22

3.4. MINOR DIRECTION ANISOTROPY ..... 24

3.5. EFFECT OF PH ..... 26

3.6. FEATURE SELECTION AND REGRESSION ..... 28

3.7. DEEP LEARNING ..... 31

4. DISCUSSION AND CONCLUSION ..... 32

REFERENCES ..... 35

II. DATA-DRIVEN OF NON-REACTIVE CONTAMINANT ATTENUATION TIME IN HETEROGENOUS POROUS MEDIA ..... 45

ABSTRACT ..... 45

1. INTRODUCTION ..... 46

2. METHODOLOGY ..... 49

2.1. POROUS MEDIA DESCRIPTION ..... 49

2.2. REACTIVE TRANSPORT MODELING ..... 51

2.3. DATA ANALYSIS ..... 53

2.3.1. Data Transformation.. ..... 53

2.3.2. Feature Selection ..... 53

3. RESULTS ..... 54

3.1. EFFECT OF PERMEABILITY STANDARD DEVIATION ..... 55

3.2. EFFECT OF FLOW ..... 57

3.3. EFFECT OF MAJOR ANISOTROPY ..... 59

3.4. EFFECT OF MINOR ANISOTROPY ..... 60

3.5. EFFECT OF TRANSVERSE DISPERSIVITY ..... 63

3.6. FEATURE SELECTION AND REGRESSION ..... 66

4. DISCUSSION AND CONCLUSIONS ..... 67

REFERENCES ..... 68

SECTION

2. CONCLUSIONS ..... 76

REFERENCES ..... 77

VITA ..... 78

# LIST OF FIGURES

Page

Paper I

Figure1. The deep neural network architecture ..... 17

Figure 2. 2D Spatial profiles of different realizations ..... 18

Figure 3. 2D Spatial profiles of different percentages of magnesite ..... 20

Figure 4. 2D spatial profiles of permeability ratio of 0.1, 1, 10 ..... 23

Figure 5. 2D spatial profiles with different major anisotropy (20 mm, 50 mm, and 100 mm) and minor anisotropy of 20 mm ..... 25

Figure 6. 2D spatial profiles of different minor anisotropy (10 mm, 20mm, 50mm) of magnesite, major anisotropy kept at 50mm ..... 27

Figure 7. 2D spatial profiles of dissolution under various inlet pH (4.0, 6.0, 8.0) ..... 29

Figure 8. Differences between actual and machine learning prediction of porosity change ..... 33

Paper II

Figure 1. 2D Spatial profiles of different realizations ..... 55

Figure 2. 2D Spatial profiles of Br transport under various standard deviations (112, 1123, 11232) ..... 58

Figure 3. Br breakthrough curves under different flow rates with low to high standard deviation ..... 59

Figure 4. 2D Spatial profiles of Br transport under various major direction anisotropy values (20, 50, 100) ..... 61

Figure 5. Br breakthrough curves for different major direction anisotropies with low to high standard deviation ..... 62

Figure 6. 2D Spatial profiles of Br transport under various minor direction anisotropy values (10, 20, 50) ..... 64

Figure 7. Br breakthrough curves for different minor direction anisotropies with low to high standard deviation ..... 65

Figure 8. Br breakthrough curves for different transverse dispersivities with low to high standard deviation ..... 65

# LIST OF TABLES

Page

Paper I

Table 1. Major and minor direction anisotropies ..... 11

Table 2. Initial and inlet conditions ..... 13

Table 3. Coefficients calculated from regression analysis ..... 30

Paper II

Table 1. Major and minor direction anisotropies ..... 50

Table 2. Initial and inlet conditions ..... 52

Table 3. Coefficients calculated from regression analysis ..... 66

# 1. INTRODUCTION

Reactive transport has a vital role in geological media from microscopic to macroscopic scale. The flow and transport regime can be significantly affected by chemical reactions such as precipitation and dissolution reactions (Berkowitz et al., 2016). Advective-dipersive-diffusive transport coupled with chemical reaction requires more complicated methods to model. The heterogeneity of natural subsurface and insufficient data make it difficult to estimate the hydraulic variables and subsequently an accurate estimation of flow and transport in natural subsurface will be difficult to attain (Wang and Huang, 2011). The goal of this study was to model the impact of heterogeneity both in reactive and non-reactive media.

## 1.1. MINERAL DISSOLUTION

The dissolution rate of a mineral can be significantly altered by physical and chemical heterogeneity. For several years, the effect of physical heterogeneity on flow and transport processes has been studied (Dentz et al., 2011a; Dentz et al., 2011b; Espinoza and Valocchi, 1998; Meile and Tuncay, 2006). However, the number of studies that have investigated the effect of chemical heterogeneties on mineral dissolution and percipitation rate are very limited (Li et al., 2007; Meile and Tuncay, 2006). The goal in this study is to quantify the reaction rate based on statistical properties of a heterogeneous porous media. Different models of the porous media were created using parameters such as mineral abundance and major and minor anisotropies. Magnesite dissolution simulations were carried out under different pH and permeability ratios (permeability of magnesite zone to sand zone). Permeability ratio, major direction anisotropy and inlet pH

were found to be the most significant variables. Most effective features were selected by lasso regression and then included in a deep learning and linear regression model in an attempt to find a model to predict mineral dissolution rate. The $R^2$ score of the linear model was only 73.2%, however 89% of the variance in the data was captured by deep learning.

## 1.2. ATTENUATION TIME OF A NON-REACTIVE CONTAMINANT

Ground water contamination has been one of the most important environmental problems for decades (Wang and Huang, 2011). Quantifying and predicting contaminant transport is crucial for ground water remediation, quality improvement and waste disposal (Gjetvaj et al., 2015; Yoon et al., 2015). Due to uneven distribution of solid materials in the natural subsurface, various spatial patterns occurs. These spatial variations lead to significant deviation in permeability of the heterogeneous porous media. The goal of this study is to quantify the transport of non-reactive contaminant in heterogeneous porous media with various spatial distribution. By using statistical parameters such as permeability standard deviation, major and minor direction anisotropies the different spatial distributions were created. Then solute transport simulations were conducted under various flow rates and transverse dispersivity values. Permeability standard deviation had the most significant impact on attenuation time. The impact of anisotropies were insignificant in low heterogeneity distribution. In contrast the effect of transverse dispersivity was only significant when heterogeneity was low. A linear regression model was created based on the features selected by lasso regression. This linear model has a $R^2$ score of 70.83%.

# PAPER

# I. PREDICTION OF MAGNESITE DISSOLUTION RATE IN HETEOGENOUS POROUS MEDIA USING DEEP LEARNING

Mahta Gholizadeh Ansari[1], Peyman Heidari[1,*], Yao Wang[1]

[1] Missouri University of Science and Technology, Department of Geosciences.

## ABSTRACT

Physical and chemical heterogeneity can significantly affect the dissolution rate of minerals in the subsurface. Two-dimensional representations of porous media were generated using statistical parameters that represent the spatial distribution of mineral. Magnesite dissolution was simulated using reactive transport modeling under various hydrogeochemical conditions. Different realizations of the porous media were generated using mineral abundance, major and minor direction anisotropies. Different permeability ratios and inlet pH were considered during the simulations. A total of 3257 simulations were carried out. The most significant variable that changed dissolution rate, porosity and concentration of $Mg^{2+}$ was permeability ratio followed by major direction anisotropy and inlet pH. More homogeneous spatial distributions have smaller anisotropy values. A more homogeneous distribution will result in higher breakthrough concentration of $Mg^{2+}$ and higher porosity change. At the end, deep learning was used to predict porosity change (reaction rate) based on statistical and hydrogeochemical parameters regardless of the underlying spatial distribution of minerals. Lasso regression was used to select features that were included in the deep learning training. The model was trained using 80% of the

data and was tested with the rest. Deep learning captured 89.0% of the variance in the test data, while a linear regression model captured only 73.2% of the variance.

## 1. INTRODUCTION

Mineral dissolution rate measurements based on field data are usually up to five orders of magnitude slower than those measured in laboratories (Maher et al., 2004; Navarre-Sitchler and Brantley, 2007; Salehikhoo et al., 2013; White and Brantley, 2003). Mineral dissolution rates have been extensively investigated both in laboratory experiments and field studies in recent decades. Most laboratory studies have been carried out in well-mixed batch or flow-through reactors. Although weathering rates have been quantified based on observed mineral depletion fronts in the field (Brantley and White, 2009; Maher et al., 2006; Zhu et al., 2009). Several reasons have been examined to understand this discrepancy, including the effect of the age of the reacting material, reaction affinity, and precipitation of secondary minerals. The goal of this study is to investigate the effects of heterogeneous distribution of physical and chemical parameters through porous media on reaction rates, and ultimately, on the discrepancy between laboratory-driven and field-scale dissolution rates. Advancing our understanding of mineral dissolution at larger scales is extremely important for precise modeling in several applications such as weathering, contaminant transport, and reactive processes in oil reservoirs.

Understanding mineral dissolution, precipitation rates, and their mechanisms is of great importance for several applications in environmental and geological systems. Over a short time scale, mineral dissolution may be responsible for adding harmful elements to

ecosystems and may also be implemented to prevent the spread of harmful elements in waste disposal and chemical remediation sites (Birkefeld et al., 2006; De Windt et al., 2004; Heidari, 2014; Mayer et al., 2002; Morrison et al., 2012; Sobanska et al., 2000; Steefel et al., 2003; Tompson and Jackson, 1996; van der Lee and De Windt, 2001; Xu et al., 2000; Yokoyama et al., 2005). Over a large time scale, mineral dissolution is the most significant process that regulates atmospheric $CO_2$ levels (Berner, 1995) and releases elements important for plant growth that sustain ecosystems (Huntington, 2000).

Numerous factors have been examined to explain the discrepancies between well-mixed laboratory rates and those measured in field studies. These include differences in the surface area of fresh and weathered minerals (Anbeek, 1993; White et al., 2005), the effect of reaction affinity (Maher et al., 2006), the precipitation of secondary minerals (Alekseyev et al., 1997; Maher et al., 2009; Moore et al., 2012; Steefel and Vancappellen, 1990) and the age of the reacting material (Maher et al., 2004; Reeves and Rothman, 2013). Recently, this discrepancy has been examined from the perspective of pore scale flow patterns and concentration alterations that are associated with it (Li et al., 2007a; Molins et al., 2012). It is known that variations in hydrological properties of porous media such as permeability lead to significant change in the flow field (Boggs et al., 1992; Heidari, 2014; Heidari and Li, 2014). These changes can significantly affect the spatial distribution of reactants in the media, which is very important during the mineral dissolution process.

Minerals in natural porous media are typically distributed unevenly with random spatial patterns, ranging from uniform distribution to clustered minerals (Allen-King et al., 1998; Barber et al., 1992; Liermann et al., 2011; Sudicky et al., 2010; Zinn and

Harvey, 2003). Various heterogeneity structures result in significant changes in statistical properties representing porous media such as permeability variance and anisotropy. Various numerical studies have identified connectivity and correlation length (anisotropy) as key parameters that determine solute breakthrough (Renard and Allard, 2013; Willmann et al., 2008). Heidari and Li (2014) have also shown that with a large enough permeability variance, the correlation length strongly controls the effective dispersivity and the extent of non-Fickian behavior when a non-reactive solute moves through a heterogeneous porous medium. Most laboratory-measured mineral dissolution reaction rates have focused on well-mixed batch reactor systems where spatial variations in abundance of the reacting phase are neglected. However, as far as we know, no study has quantified reaction rates based on the statistical properties of porous media. In addition, fluid flow and transport are neglected by nature in the well-mixed reaction rate measurements (Li et al., 2007a). In the subsurface, however, the reaction, fluid flow and transport occur simultaneously.

Although the effect of physical heterogeneity on flow and transport processes has been studied for several decades, chemical heterogeneity has attracted much less attention (Dentz et al., 2011a; Dentz et al., 2011b; Espinoza and Valocchi, 1998; Meile and Tuncay, 2006). Moreover, the number of studies that have investigated the effect of chemical heterogeneties on mineral dissolution and percipitation rate are very limited (Li et al., 2007a; Meile and Tuncay, 2006). Pore-scale modeling studies have shown that spatial distribution of Anorthite in porous media resulted in a factor of 3 lower overall rates, even with the same amount of mineral (Li et al., 2006, 2007b). The majority of the studies on the effect of spatial distribution of mineral in porous media on mineral

dissolution rates have focused on modeling (Li et al., 2011; Li et al., 2006, 2007b) except for a few studies (Li et al., 2014; Salehikhoo et al., 2013; Smith et al., 2013).

In recent years, Artificial Neural Networks (ANN) have been widely used for modeling water resources in environmental sciences such as water quality (Gümrah et al., 2000; Maier and Dandy, 1998), water resources and management (Coppola et al., 2003; Gaur et al., 2013; Maier and Dandy, 1998; Nikolos et al., 2008; Rizzo and Dougherty, 1994; Tsai et al., 2016) optimizing remediation (Rizzo and Dougherty, 1996; Rogers and Dowla, 1994; Yan and Minsker, 2006), run-off prediction (Piotrowski et al., 2016), solute transport in groundwater (Almasri and Kaluarachchi, 2005; Lischeid et al., 2003; Luciano et al., 2013; Morshed and Kaluarachchi, 1998a, b) and permeable reactive barriers (Guruprasad et al., 2011). Morshed et al. (1998a) used ANN to predict breakthrough curves (BTC) based on flow and transport parameters. The main parameters of breakthrough curves are breakthrough time, the time at which the maximum contaminant level (MCL) has been reached and maximum concentration. In their study, the applicability of ANN was assessed for simulating these parameters as functions of flow, transport and combination of the two. Based on their findings, ANN can simulate the effects of flow with an $R^2$ of 0.99, the effect of transport with an $R^2$ of 0.985, and the effect of both flow and transport with an $R^2$ of 0.998 on the four main parameters of BTC. The number of hidden layers of most of these neural networks is limited due to computational cost required to train deep networks. Due to advances in algorithms and the emergence of powerful CPUs, deep (multi-layered) neural networks have recently won numerous machine learning contest recently (Schmidhuber, 2015). In the area of environmental sciences, Song et al. (2016) have shown that deep belief nets (Hinton et

al., 2006) could highly contribute to enhancing the soil moisture estimations. However, this technique has not yet been implemented to predict mineral dissolution to the best of our knowledge.

In this study, we propose to study the relationship between statistical parameters representing "small-scale" heterogeneities in porous media and "large-scale" mineral dissolution rates. We intend to quantify reaction rate based on transport limitations and local heterogeneities. In addition, we will use machine learning to examine the possibility of predicting mineral dissolution rate using deep learning (LeCun et al., 2015).

## 2. METHODOLOGY

### 2.1. MAGNESITE DISSOLUTION

Three parallel reactions have been proposed for magnesite dissolution (Chou et al., 1989; Plummer et al., 1978; Salehikhoo and Li, 2015)

$$MgCO_3 + H^+ \leftrightarrow Mg^{2+} + HCO_3^- \quad (1)$$

$$MgCO_3 + H_2CO_3 \leftrightarrow Mg^{2+} + CO_3^{2-} \quad (2)$$

$$MgCO_3 \leftrightarrow Mg^{2+} + CO_3^{2-} \quad (3)$$

According to Transition State Theory (TST), the magnesite dissolution rate can be calculated as (Li et al., 2014):

$$R_{MgCO_3} = \left(k_1 \times a_{H^+} + k_2 \times a_{H_2CO_3} + k_3\right) \times \mathrm{A} \times \left(1 - \frac{IAP}{K_{eq}}\right) \quad (4)$$

$$IAP_{MgCO_3} = a_{Mg^{2+}} \times a_{CO_3^{2-}} \quad (5)$$

where R represents the overall rate for magnesite; and $k_1, k_2, k_3$ (mol/$m^2$/s ) are the rate constants of reaction (1)-(3); the values used in this study in Equation (4) are $2.5\times10^{-5}$, $6\times10^{-6}$ and $4.5\times10^{-10}$, respectively (Chou et al., 1989); $A$ is the surface area of a

mineral; $a_i$ stands for the activities of aqueous species; IAP is the ion activity product of $a_{Mg^{2+}}$ and $a_{CO_3{}^{2-}}$, defined in Equation (5); $K_{eq}$ is the equilibrium constant for Equation (3); and $logK_{eq}$ is -8.234 (Wolery et al., 1990); So $\frac{IAP}{K_{eq}}$ represents the distance from equilibrium. Under different circumstances, each of these three rate constants can have a relatively significant effect on the overall reaction rates. In acidic conditions, the rate of the first reaction is proven to be the most important. If the concentrations of $CO_2$ are high, the second reaction rate is the controlling one and the third rate is the most effective when pH conditions is more alkaline (pH higher than 6-7) (Li et al., 2014).

## 2.2. POROUS MEDIA DISCRIPTION

This study has a numerical approach to investigate the effects of heterogeneous distribution of physical and chemical parameters through porous media on dissolution rates of magnesite. The dimensions of the quasi-2D porous medium is 200mm×200mm×1mm. The modeling domain consists of 40,000 grid blocks of 1mm×1mm×1mm. Three different combinations of percentages of magnesite and sand are considered in this work: 90% sand to 10% magnesite, 70% sand to 30% magnesite, and 50% sand to 50% magnesite. Spatial distributions of minerals in porous media were determined using a commercial software, PETREL from Schlumberger. PETREL is a software capable of building porous media models, interpreting seismic data, and performing well correlation, which is normally used in the oil and gas industry (Gringarten and Deutsch, 2001). To produce a 2D realization of the porous medium, PETREL requires major and minor direction anisotropies, a variogram model, and sand and magnesite percentages.

Variograms are widely used in geostatistical analysis to describe the spatial relationship between values of a parameter (Webster and Oliver, 1993). The variogram equation is as follows (Gringarten and Deutsch, 2001; Warrick and Myers, 1987):

$$2\gamma(\mathrm{h}) = \mathrm{E}[\mathrm{Y}(\mathrm{u}) - \mathrm{Y}(\mathrm{u}+\mathrm{h})]^2 \qquad (6)$$

where *Y* represents a stationary random function (the type of mineral in this study) and $h$ stands for a distance vector. In other words, the variogram defines the expected square difference for different data with a distance vector of $h$ (Gringarten and Deutsch, 2001). We can also use a semivariogram $\gamma(h)$, which is half of the variogram, $2\gamma(h)$. A semivariogram is described by several characteristics. Theoretically, a semivariogram's value at the origin should be zero, whenever it is anything other than zero the value at the origin is referred to as the nugget, which can represent measurement error (Bohling, 2005; Gringarten and Deutsch, 2001; Manto, 2005). The sill ( $\gamma_\infty$) describes the variance of the random field and neglects the spatial structure (Gringarten and Deutsch, 2001; Manto, 2005). Range is the distance at which sill is reached by the semivariogram (Bohling, 2005). Another name for range is anisotropy, which is used in this study. Here, the values for the nugget and sill are 0.0001 and 1.0, respectively.

The most commonly studied variogram models are those with a sill, such as a spherical model, exponential model, Gaussian model or nugget model (Bohling, 2005; Gringarten and Deutsch, 2001; Warrick and Myers, 1987). In addition, if a semivariogram value changes due to changes of the direction, it is called an anisotropic varigoram (Manto, 2005). For the purpose of this study an exponential anisotropic variogram was chosen, because the exponential model is considered more appropriate for representating of high variability with lower range (Bohling, 2005). For the purpose of

geo-modeling, PETREL accepts mineral percentage, porous media geometry, variogram model, and major and minor direction anisotropies. Fourteen different pairs of major and minor direction anisotropies were chosen for this study as shown in Table 1. After providing all required inputs, the software will randomly generate a spatial distribution honoring all parameters. However, there are numerous distributions that will honor these restriction. Therefore, ten different realizations were generated for each simulation case (for example, 50% sand to 50% magnesite, major direction anisotropy=50 mm, major direction anisotropy=50 mm) to reduce the effect of any specific spatial distribution.

Table 1. Major and minor direction anisotropies

| Combination | Major(mm) | Minor(mm) | Combination | Major(mm) | Minor(mm) |
|---|---|---|---|---|---|
| **Case 1** | 1 | 1 | **Case 8** | 50 | 10 |
| **Case 2** | 10 | 1 | **Case 9** | 50 | 20 |
| **Case 3** | 10 | 10 | **Case 10** | 50 | 50 |
| **Case 4** | 20 | 1 | **Case 11** | 100 | 1 |
| **Case 5** | 20 | 10 | **Case 12** | 100 | 20 |
| **Case 6** | 20 | 20 | **Case 13** | 100 | 50 |
| **Case 7** | 50 | 1 | **Case 14** | 100 | 100 |

## 2.3. REACTIVE TRANSPORT MODELING

The aqueous concentrations are determined by flow and transport processes in addition to the geochemical reaction systems. In a system with magnesite dissolution as

the sole kinetically controlled reaction, the governing reactive transport equation is as follows (Salehikhoo and Li, 2015):

$$-\frac{\partial(C_{Mg(II)})}{\partial t} = \nabla.(-D\nabla C_{Mg(II)} + vC_{Mg(II)}) + R_{MgCo3} \qquad (7)$$

where $C_{Mg(II)}$ is the total $Mg^{2+}$ concentration (mol/m$^3$), $t$ is the time (s), $D$ is the combined dispersion–diffusion tensor (m$^2$/s), $v$ is the flow velocity vector (m/s), and $R_{MgCO_3}$ is the magnesite dissolution rate (mol/s) calculated from a Transition State Theory (TST) based rate law (Salehikhoo and Li, 2015). If the numerical simulation resolution is high enough, we can assume a well-mixed condition in each grid block. Therefore, simulation is carried out using a TST rate law from a batch experiment to calculate $R_{MgCO_3}$ (Chou et al., 1989). In recent studies, it has been observed that magnesite dissolution rates decreased from an evenly distributed pattern to clustered parallel to main flow direction layer (Li et al., 2014; Salehikhoo et al., 2013).

All the numerical simulations were carried out using CrunchFlow, a pertinent code for geochemical modeling of reactive transport processes in the subsurface (Heidari and Li, 2014; Li et al., 2011; Maher et al., 2009; Singha et al., 2011; Steefel et al., 2003; Steefel and Lichtner, 1994). The following species are involved in aqueous reactions: $Mg^{2+}, MgHCO_3^-, MgCO_3(aq), Cl^-, H_2CO_3, HCO_3^-, CO_3^{2-}, H^+, OH^-, Na^+, K^+, Br^-$. Here, primary species are: $Mg^{2+}, HCO_3^-, H^+, Na^+, K^+$ and $Br^-$ the rest are secondary species (Li et al., 2014; Salehikhoo et al., 2013). The code solves for concentration of each primary species by numerically approximating Equation (7) and uses equilibrium constants to calculate secondary species. The initial and inlet conditions for magnesite dissolution are shown in Table 2. All simulations were performed with 35% porosity and a flow rate of 5 ml/min, with longitudinal and transverse dispersivity of

0.05 and 0.005 (cm), respectively (Heidari and Li, 2014). In addition to the effect of magnesite abundance, magnesite spatial distribution, and anisotropy, the effect of permeability variance (permeability ratio) between the sand and magnesite zones on mineral dissolution were examined. For permeability ratios (permeability of magnesite divided by permeability of sand), values of 10, 1 and 0.1 were chosen. Under conditions where the permeability ratio was 1 both zones had a permeability value of $1 \times 10^{-13}$ $m^2$. Moreover, to examine the effect of inlet fluid on magnesite dissolution, three pH values (4, 6 and 8) were considered. For each of the treatment combinations mentioned above, simulations were run for all unique spatial distributions obtained from PETREL. A total of **3527** simulations were obtained and each simulation took 2 - 12 hours to complete.

Table 2. Initial and inlet conditions

| Species | Inlet condition(mol/l) | Initial conditions(mol/l) |
|---|---|---|
| **pH** | 4.0 or 6.0 or 8.0 | 8.0 |
| **SiO2(aq)** | 1.0E-9 | 1.0E-9 |
| **CO2(aq)** | 1.2581E-9 | 1.2581E-9 |
| **$Br^-$** | 1.00E-4 | 1.0E-7 |
| **$Na^+$** | 1.0000E-3 | 1.0000E-3 |
| **$Ca^{2+}$** | 1.2581E-9 | 1.2581E-9 |
| **$Cl^-$** | 1.0000E-3 | 1.0000E-3 |
| **$Mg^{2+}$** | 1.2581E-9 | 1.0E-7 |

## 2.4. MACHINE LEARNING

Results of a total of 3527 simulation cases were analyzed to calculate the porosity increase in each case. Porosity increase was solely attributed to magnesite dissolution (sand is relatively non-reactive). Machine learning was used to train models that predict porosity change based on statistical parameters that represent hydrogeochemical condition of the dissolution process. In order to more reliably measure accuracy of the trained model, the data was randomly divided into three datasets: the training dataset (80%), validation dataset (10%), and test datasets (10%). Each model was then trained on the training dataset. Then, the models were fine-tuned on the validation dataset. Finally, the models were tested for accuracy on the test dataset and their accuracy was reported. The accuracy metric in this study is $R^2$. During training, each model tries to minimize a loss value. Here, the loss value is the sum of squared error between the predicted porosity change using machine learning and the calculated porosity change using numerical simulation.

**2.4.1. Feature Selection.** In this study, the changes of porosity was chosen to be the dependent variable. The permeability ratio of magnesite to sand, pH, magnesite percentage, permeability of magnesite, and major and minor direction anisotropy were the independent variables. In order to establish some non-linear features based on the independent variables, each variable was transformed using the following non-linear functions: $x^2,\ x^3,\ x^4,\ \frac{1}{x}, 10^x, 10^{-x},\ log\ (x), ln(x), \sqrt[2]{x}, \sqrt[3]{x}$. Therefore, each case started with 6 features that were turned into 66 features using this transformation.

In order to select the features, the least absolute shrinkage and selection operator (Lasso) regression method was chosen. Lasso regression is a method proposed by

Tibshirani to address the short comings of subset selection and ridge regression (Tibshirani, 1996). In subset selection, even slight changes in data will result in a significant change in the selected models, thus having a negative impact on the accuracy of the estimation (Frank and Friedman, 1993; Tibshirani, 1996). Even though ridge regression shrinks some of the coefficients (Hoerl and Kennard, 2004) it does not necessarily assign 0 to any coefficient, which makes it difficult to select the most effective independent variable (Tibshirani, 1996). Lasso regression has been commonly used for variable selection (Meinshausen and Bühlmann, 2006; Zhao and Yu, 2006; Zou, 2006). Lasso regression enforces a penalty in the form of the absolute value of the coefficients, the algorithm continues to reduce the coefficients and assign a coefficient of zero to some of the variables, which makes variable selection more convenient than in many other methods (Jahreis, 2015; Tibshirani, 1996; Zou and Hastie, 2005). Lasso estimates are regulated by a penalty parameter called λ. For λ value of zero, the lasso estimator will be the same as an ordinary least squares estimator that minimizes the residuals. In contrast, large values of λ will shrink all the coefficients to zero (Jahreis, 2015). Choosing a moderate λ is vital for proper variable selection. Using a cross validation method can simplify the procedure of choosing a proper λ value (Hastie, 2009).

**2.4.2. Deep Learning.** Artificial neural networks (ANN), which were originally inspired by biological nerve system interconnections, are mathematical models that are capable of unfolding complex relationships (Guruprasad et al., 2011; McCulloch and Pitts, 1943).

ANN consists of multiple units resembling neurons, which produce an output based on a given input value and its activation functions (Almasri and Kaluarachchi, 2005). The weight values of the activation function are representative of the interconnections between the units (Yan and Minsker, 2006). Modification of the weights related to each of these interconnections leads to a learning algorithm capable of demonstrating the relationship between outputs and inputs (Yan and Minsker, 2006). The back propagation algorithm was first introduced by Rumelhart (Rumelhart, 1986). This algorithm has two general procedures to find the weight vector ($\boldsymbol{w}$). Initially, it assigns small random variables to w. Then, it updates these values using the training dataset to minimize the mean square error (Almasri and Kaluarachchi, 2005).

Here, we trained a deep neural network (Bengio, 2009; Deng and Yu, 2014) using the back propagation algorithm. The network architecture can be seen in Figure 1. There were a total of 14 hidden layers. The input layer had 20 nodes, which correspond to features for each case that were selected using Lasso regression. Immediately after the input layer, there are two linear hidden layers with 64 nodes each. After these layers, there are eight linear hidden layers with 128 nodes each. After these, there are two tanh (hyperbolic tangent) hidden layers with 128 nodes each followed by two sigmoid (logistic) hidden layers with 128 nodes each. Finally, there is a one-node linear output layer. In addition to weights and biases between layers, the number of layers, nodes per layer, and type of activation function in each layer were selected during the training process using the training and validation datasets. It should be mentioned that no over fitting was observed during the training process.

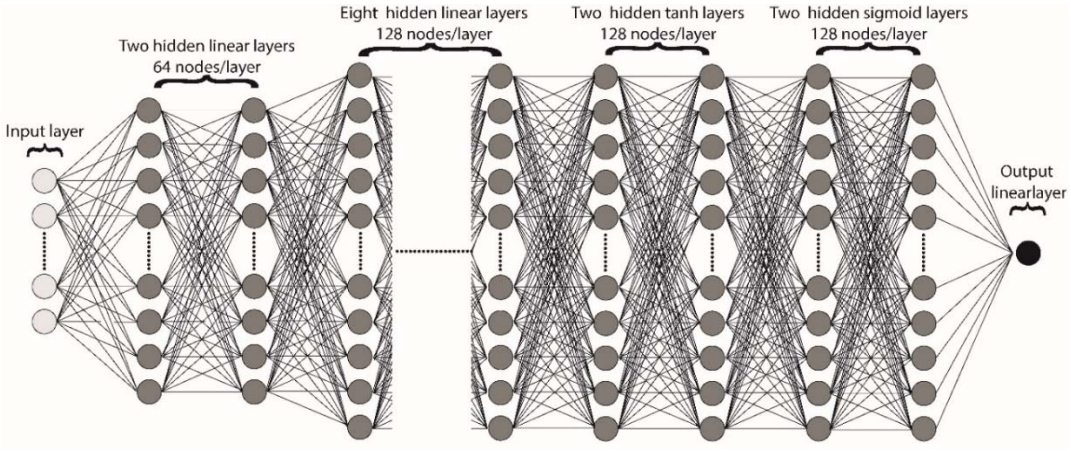


Figure1. The deep neural network architecture

## 3. RESULTS

To demonstrate the extent of variability among the realizations, three random realizations were chosen out of the ten simulation sets for 30% magnesite and 70% sand with major and minor anisotropy directions of 50 mm and 20 mm, respectively. The simulations all had the same conditions, with an inlet pH of 8 and a permeability ratio of 1. As shown in Figure 2, even though the mineral spatial distribution is significantly different, the reaction rates or saturation indices are not significantly different from one another. Figure 2 (j) - (l) show that there is only a slight difference in the $Mg^{2+}$ concentration, porosity and overall rate for different realizations. Figure 2 demonstrates that the small scale distribution might not be a significant factor in determining reactive transport processes if all statistical parameters are the same.

### 3.1. MAGNESITE ABUNDANCE

The effect of magnesite abundance (percentage) on dissolution rate was examined. Figure 3 (a)–(c) shows the spatial distribution of magnesite and sand in three

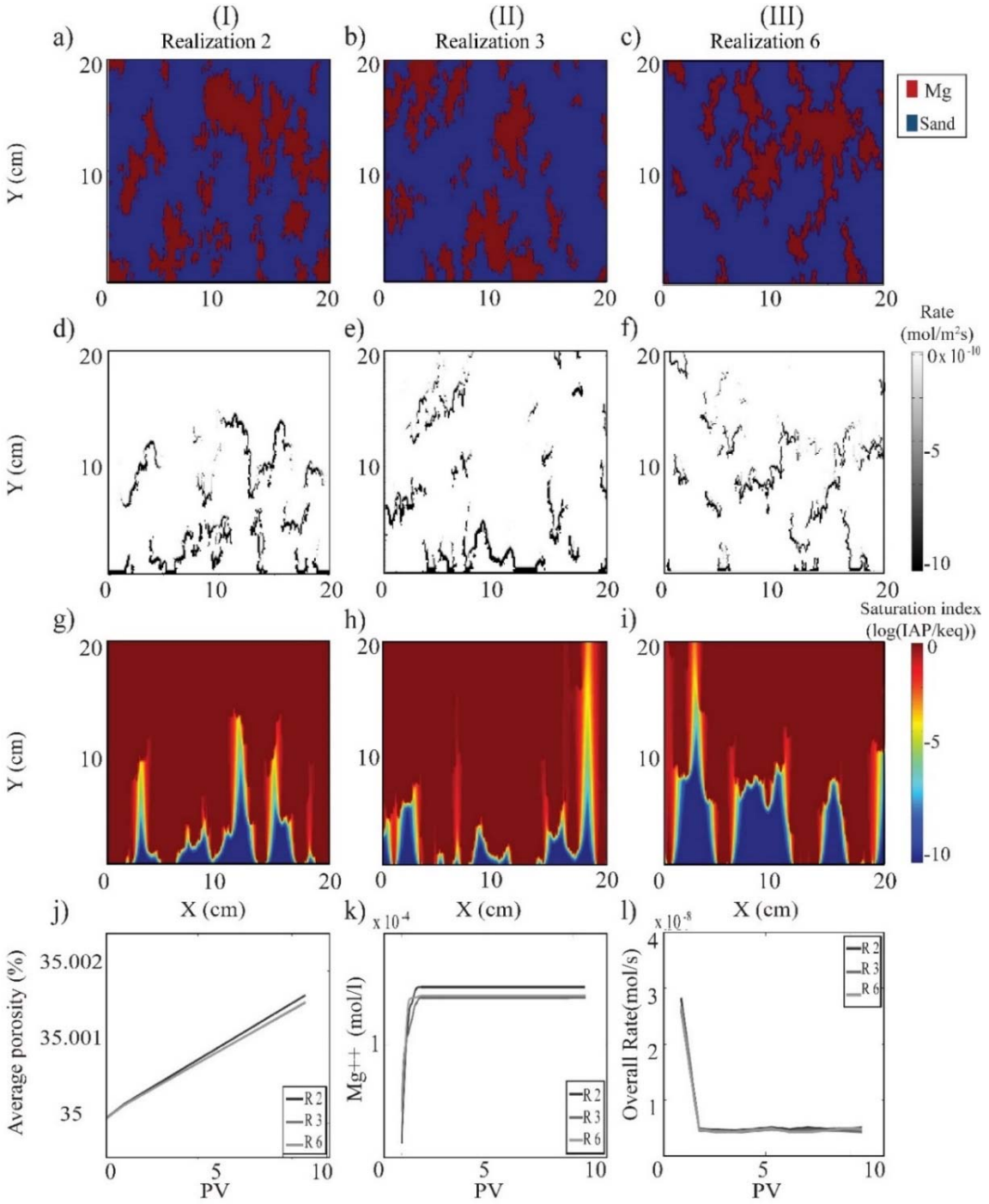


Figure 2. 2D Spatial profiles of different realizations: (a)–(c) the spatial distribution of sand and magnesite, (e)–(h) magnesite reaction rate under steady-state condition, and (g)–(i) saturation index of pore solution under steady state condition. j) average porosity change, k) concentration of Mg2+. l) overall rate of magnesite dissolution.

randomly selected cases. In columns (I) through (III), the percentage of magnesite increases from 10% to 50%. Figure 3 (d)–(f) shows the magnesite dissolution rate, with the black portion of the figure specifying the high reaction rate zones. As expected (Figure 3 (d)–(f)), the lowest percentage of magnesite had the lowest reaction rate. Figure 3 (g)–(i) shows the natural log of the saturation index of the pore solution. Note that a zero saturation index indicates an equilibrium condition, so a higher percentage of magnesite had a saturation index closer to the equilibrium. However, the spatial distributions of saturation indexes of the 30% and 50% magnesite cases are comparable. Figure 3 (j)–(l) demonstrate change of variables over time. We analyzed ten realization, plotting the average between the ten values and the standard deviation between values as error bars. Figure 3 (j) shows that the average porosity increased with the increase in percentage of magnesite; however, it does not show a very distinguishable change in porosity when the percentage of Mg increases from 30% to 50%. Figure 3. (k) shows the overall breakthrough curve of $Mg^{2+}$ for different percentages of magnesite. With the increase in percentage of magnesite, the concentration of $Mg^{2+}$ also increased, and there was a significant change from 10% to 30% of magnesite, but just a slight declination when the porous media magnesite percentage increased from 30% to 50%. In Figure 3 (l), the overall rate increased with the percentage of magnesite increase, but the change was not significant. Increase in abundance of magnesite results in an increase in dissolution rate. However, the changes are more pronounced with increase from 10% to 30% compared to increase from 30% to 50%. Increase of abundance leads to a higher percentage of pores being occupied with reactant minerals. Therefore, the porosity, effluent $Mg^{2+}$ concentration and overall dissolution rate increase.

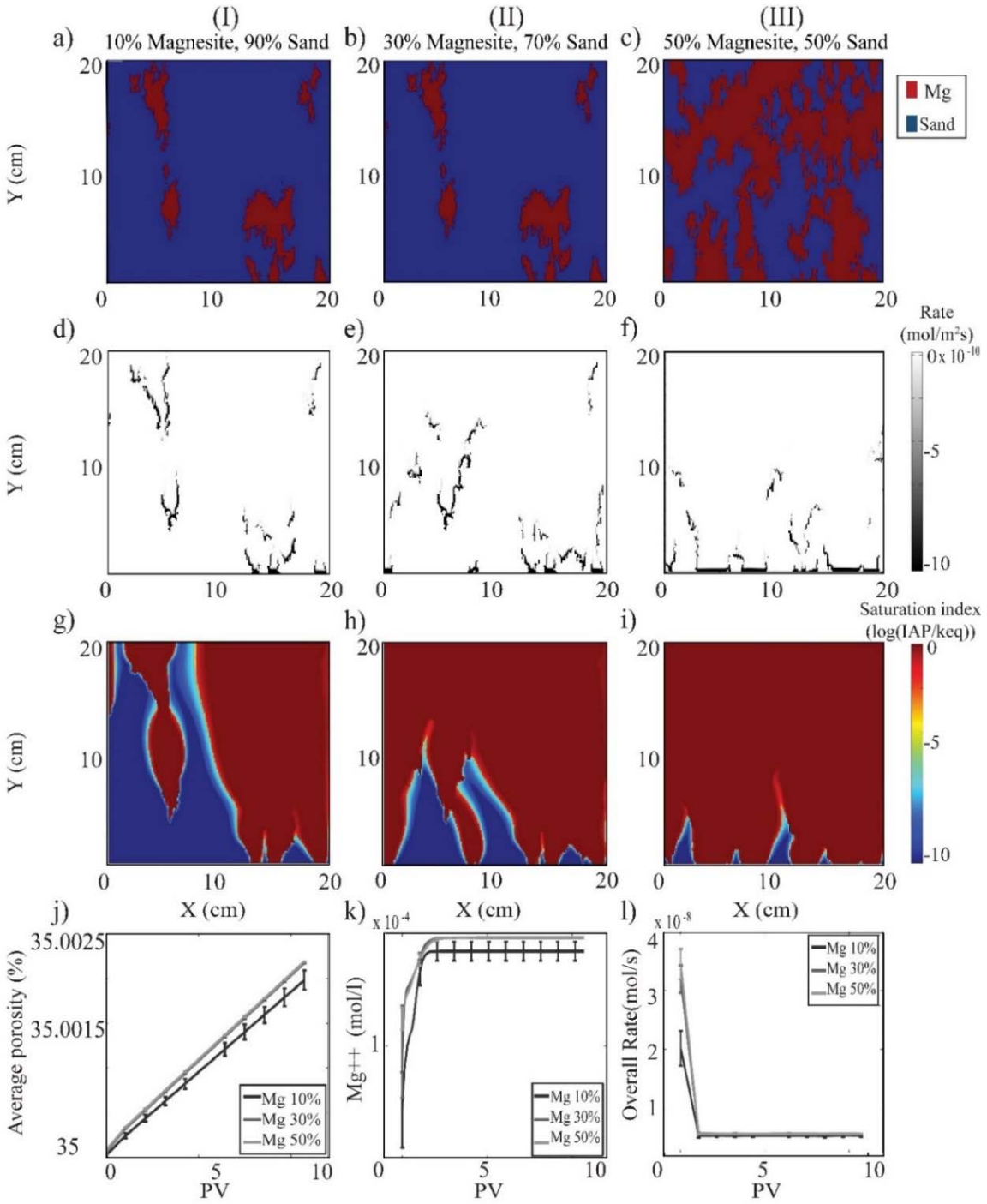


Figure 3. 2D Spatial profiles of different percentages of magnesite: (a)–(c) show spatial distribution of sand and magnesite, (e)–(h) magnesite reaction rate under steady-state conditions, with the black zones indicating the highest reaction rates and (g)–(i) the natural log of saturation index of the pore solution. j) average porosity, k) concentration of Mg2+ and l) overall rate of dissolution of magnesite. The lines in (j)–(l) are average and error bars are standard deviation of ten different realizations.

Moreover, saturation index increases in magnesite zones towards the outlet. As shown in the reaction rate spatial distribution in Figure 3. (d)-(e), the local reaction rate in zones that have reached equilibrium are significantly lower than the inlet or magnesite-sand interface. It can be concluded that effective dissolution occurs only for magnesite grains on the sand-magnesite interface, and magnesite grains deeper in the magnesite zone will not react because the pore solution is already at equilibrium, as shown in Figure 3. (g)-(i) (Li et al., 2014). Figure 3. (j)-(k) indicates that there is a significant change in porosity, $Mg^{2+}$ concentration and overall rate when percentage of magnesite increases from 10% to 30%. However, the changes in those values are relatively trivial when magnesite abundance is set to 50%. This indicates that increase in abundance above a certain limit might not lead to a significant increase in reaction rate because reactions mostly occur on the reactive zones interface and the size of the reactive zone does not significantly affect dissolution rates (Li et al., 2007a).

### 3.2. PERMEABILITY RATIO

The effect of difference in permeability between the reactive zone and the non-reactive zone was studied. Figure 4 (a)–(c) shows the three spatial distributions of minerals with the permeability ratios of magnesite-to-sand zones of 10, 1 and 0.1. These cases were randomly selected for visualization. Figures 4 (d)–(f) shows the magnesite dissolution rate where the black zones of the distribution indicate the highest reaction rates. Based on this visualization, reaction rates are comparable. Figure 4 (g)–(i) illustrates the saturation index of pore solution, where higher permeability of magnesite has wider zone approaching equilibrium conditions. The higher the permeability of the

magnesite zone, the closer the results are to equilibrium. The overall breakthrough curve shown in Figure 4 (k) demonstrates that $Mg^{2+}$ concentration increases with increase of the magnesite zone permeability.

In cases where permeability of magnesite is 1 order of magnitude higher than the permeability of sand, a higher portion of the inlet solution flows through the reactive zone, which results in higher reaction rates and higher breakthrough concentrations (Figure 4, column I). In contrast, fluid flow is mostly through the nonreactive zone due to lower permeability in the reactive zone, as shown in Figure 4 (column III). The low flow rate through the reactive zone limits mass transport and subsequently decreases reaction rate (Molins et al., 2012; Salehikhoo and Li, 2015). In other words, when aqueous phase concentration is near-equilibrium, the rate-limiting process in the overal reaction rate of the porous media is transport rather than rate of geochemical detachment from the surface of the mineral (Berner, 1981; Steefel, 2009). As shown in Figure 4 (j)-(k), increasing the permeability of the reactive zone by two orders of magnitude will result in an increase of $Mg^{2+}$ concentration, porosity and overall rate by a factor of two.

### 3.3. MAJOR DIRECTION ANISOTROPY

Anisotropy (variogram range) is a directional variable. In this section, the effect of major direction anisotropy on mineral dissolution was studied. Figure 5 (a)–(c) demonstrates the 2D spatial distribution of the porous media consisting of 10% magnesite and 90% sand. To illustrate the effect of major anisotropy, minor anisotropy was kept constant at 20 mm and major anisotropy values was set to 20, 50, and 100 mm.

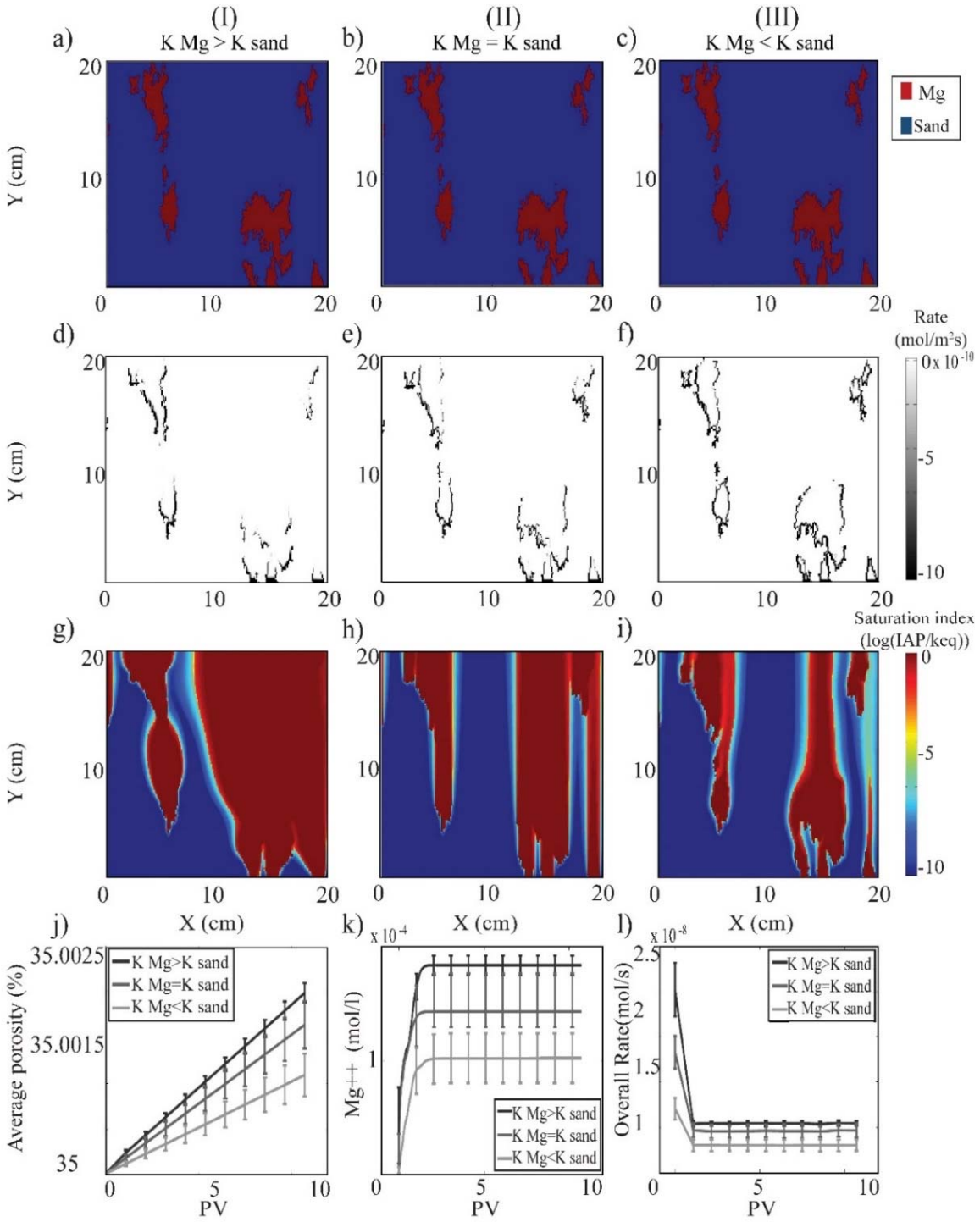


Figure 4. 2D spatial profiles of permeability ratio of 0.1, 1, 10: (a)–(c) the spatial distribution of minerals (Mg is shown as red and sand as blue); (d)–(f) the magnesite reaction rate; (g)–(i) saturation index of pore solution. j) average porosity, k) concentration of Mg2+ and l) overall rate of dissolution of magnesite. The lines in (j)–(l) are average and error bars standard deviation of ten different realizations.

Figure 5 (d)–(f) shows the magnesite dissolution rate distribution, where lower major anisotropy shows a relatively uniformly distributed reaction profile along the flow direction. Similarly, the pore solution saturation index with respect to magnesite dissolution demonstrates that pore water chemistry moves further away from the equilibrium condition as the major anisotropy increases, as shown in Figure 5 (g)–(i).

Increase of major direction anisotropy results in aggregation of reactive particles along the flow direction. Therefore, as the major direction anisotropy decreases the spatial distribution moves toward a more homogeneous distribution. More homogeneously distributed minerals leads to higher dissolution rate, larger equilibrium zone, and higher rate of porosity increase (Figure 5). Because reactions occur mostly on the reactive zone interface with the non-reactive zone, smaller anisotropy increases the interface contact area and a larger portion of the reactive zone will be in contact with far-from-equilibrium inlet solution.

### 3.4. MINOR DIRECTION ANISOTROPY

In addition to major direction anisotropy, the effect of minor direction anisotropy on mineral dissolution was also studied. The minor direction is the direction perpendicular to the flow.

Figure 6 (a)–(c) illustrate the 2D spatial distribution of magnesite and sand with different minor anisotropy values. From left to right, the minor anisotropy increases from 10 mm to 50 mm. Major direction anisotropy is constant at 50 mm for all cases. As shown in Figure 6 (g)-(i), increase of minor direction anisotropy causes the solution to move slightly further away from the equilibrium conditions.

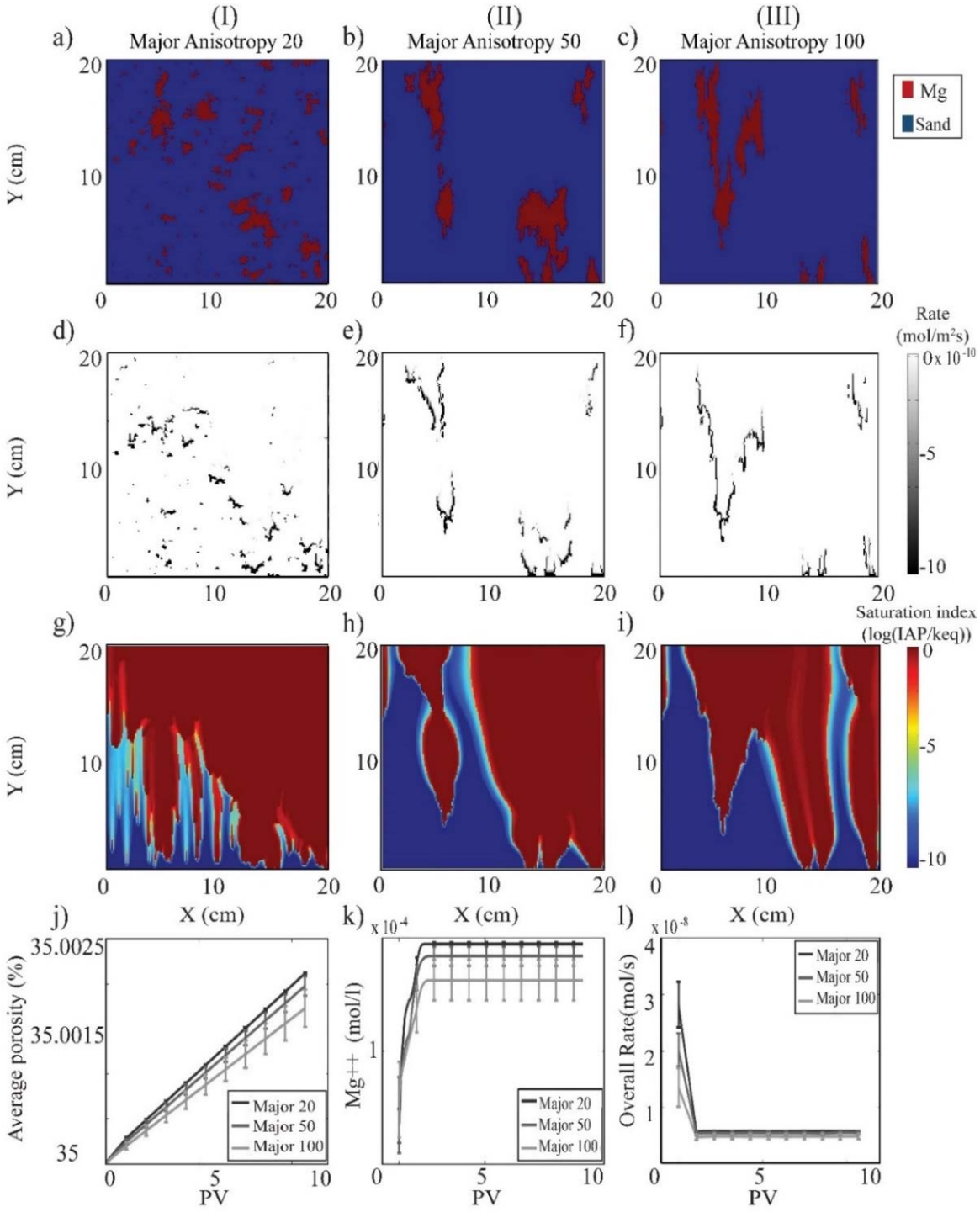


Figure 5. 2D spatial profiles with different major anisotropy (20 mm, 50 mm, and 100 mm) and minor anisotropy of 20 mm: (a)–(c) the spatial distribution of minerals; (d)–(f) the magnesite reaction rate; (g)–(i) saturation index of pore solution. j) average porosity, k) concentration of Mg2+ and l) overall rate of dissolution of magnesite.

Therefore, increase of minor anisotropy is associated with negligible reduction in average porosity and effluent $Mg^{2+}$ concentration as shown in Figure 6 (j)–(k).Theoretically, lower values of minor direction anisotropy should lead to higher reaction rates. It should be mentioned that these results might be affected by our choice of major direction anisotropy and magnesite abundance.

Different minor and major anisotropy will help us compare the effect of chemical heterogeneity and its spatial distribution in porous media on overall porosity change and reaction rate. With lower anisotropy values, the porous media resembles a well-mixed condition (Li et al., 2011; Li et al., 2014) or chemically homogeneous porous media; therefore, reaction is almost uniformly distributed in the system. In a physically homogeneous condition, it is assumed that each magnesite grain is in contact with the sand, which results in relatively higher reactive surface areas compared to a cluster of magnesite in a sand zone (Li et al., 2014). It is assumed that dissolution is happening all over the porous media, which leads to higher $Mg^{2+}$ concentration and IAP/keq values along the flow direction. Interestingly, major anisotropy values have a more significant impact on the steady state $Mg^{2+}$ concentration, porosity and rate.

### 3.5. EFFECT OF PH

To understand the effect of inlet pH on reaction rates in heterogeneous porous media, three cases were randomly selected to be analyzed in Figure 7. All other variables were constant, while the only difference is inlet pH was set to 4.0, 6.0, and 8.0. Figure 7 (g)-(i) shows the saturation index of pore solution. Pore solution saturation index reached equilibrium condition in all pH values.

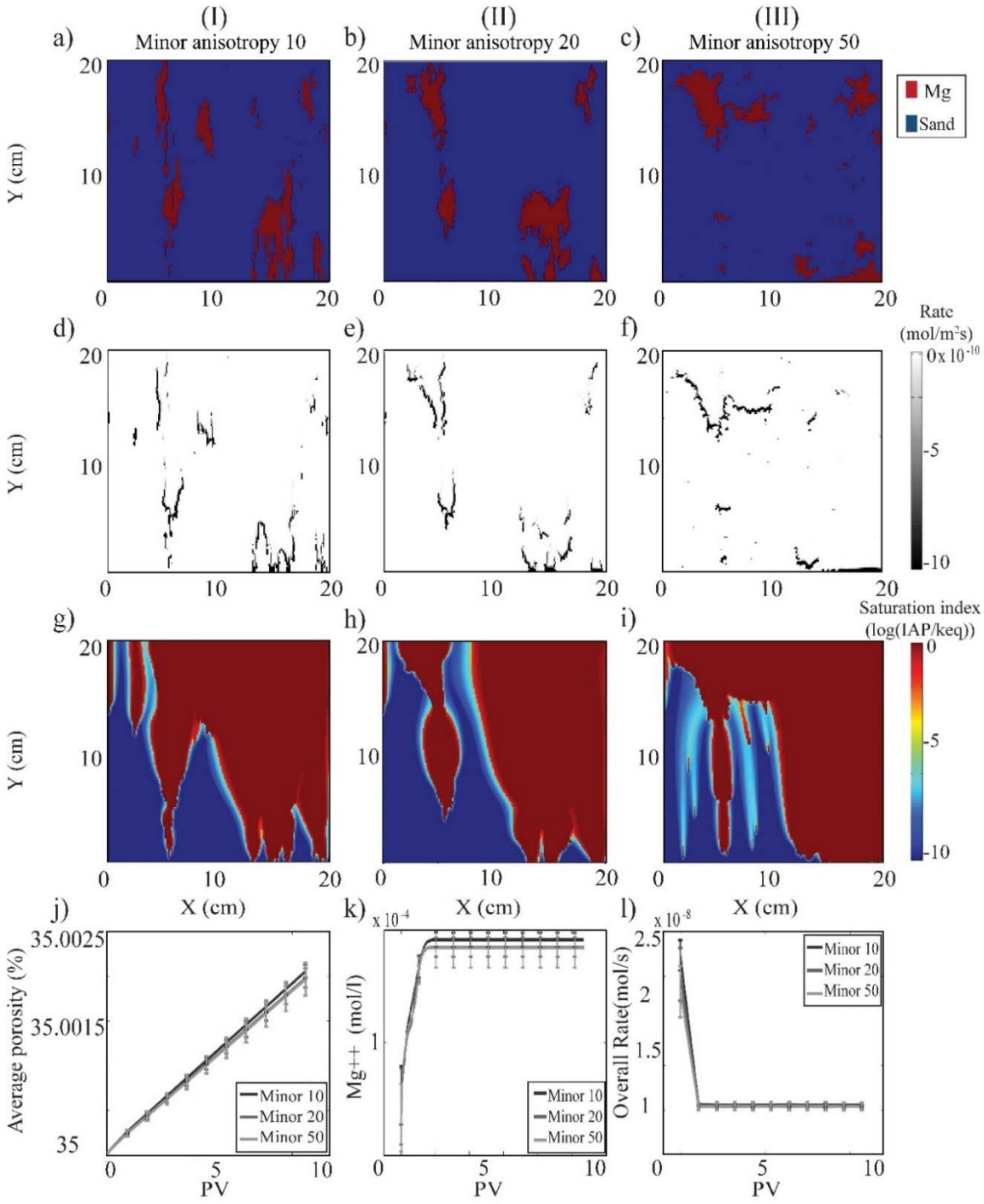


Figure 6. 2D spatial profiles of different minor anisotropy (10 mm, 20mm, 50mm) of magnesite, major anisotropy kept at 50mm: (a)-(d) the spatial distribution of mineral; (e)-(h) magnesite dissolution rate, and (i)-(l) saturation indexes of pore solution. j) average porosity, k) concentration of Mg2+. l) overall rate of dissolution of magnesite.

However, the equilibrium condition was different for each case due to different chemical conditions. In pH 6.0 and 8.0, similar to acidic condition (pH=4.0), equilibrium was reached within the magnesite zone, but in the immediate vicinity of magnesite-sand interface, log IAP/keq gradually became smaller than zero and moved further from the equilibrium. In other words, the transient zone between local equilibrium and far from equilibrium became wider.

Interestingly, there is a significant decrease in $Mg^{2+}$ concentration in Figure 7 (j)-(l) and increase in porosity change due to pH increase from 4.0 to 6.0, but the changes are trivial when pH value is raised to 8.0. At 25℃ magnesite dissolution rate is highly dependent on pH and has a linear relationship with $H^+$ activity in mild acidic solutions (3.0<pH<5.0) (Chou et al., 1989; Pokrovsky et al., 2009). In addition, Pokrovsky et al. (1999) stated that dissolution rate is independent of pH values within the range of 5.0 to 8.0, which corresponds well with our findings. Our results are in agreement with the previous findings even though our simulations were carried out in heterogeneous porous media.

## 3.6. FEATURE SELECTION AND REGRESSION

The change of porosity was chosen to be the dependent variable and permeability ratio of magnesite to sand, pH, magnesite percentage, permeability of magnesite, major and minor direction anisotropies were the independent variables. In order to establish some non-linear variables based on our initial variables, the functions, $x^2, x^3, x^4, \frac{1}{x}, 10^x, 10^{-x}, log\ (x), ln(x), \sqrt[2]{x}, \sqrt[3]{x}$ were used to transform the data.

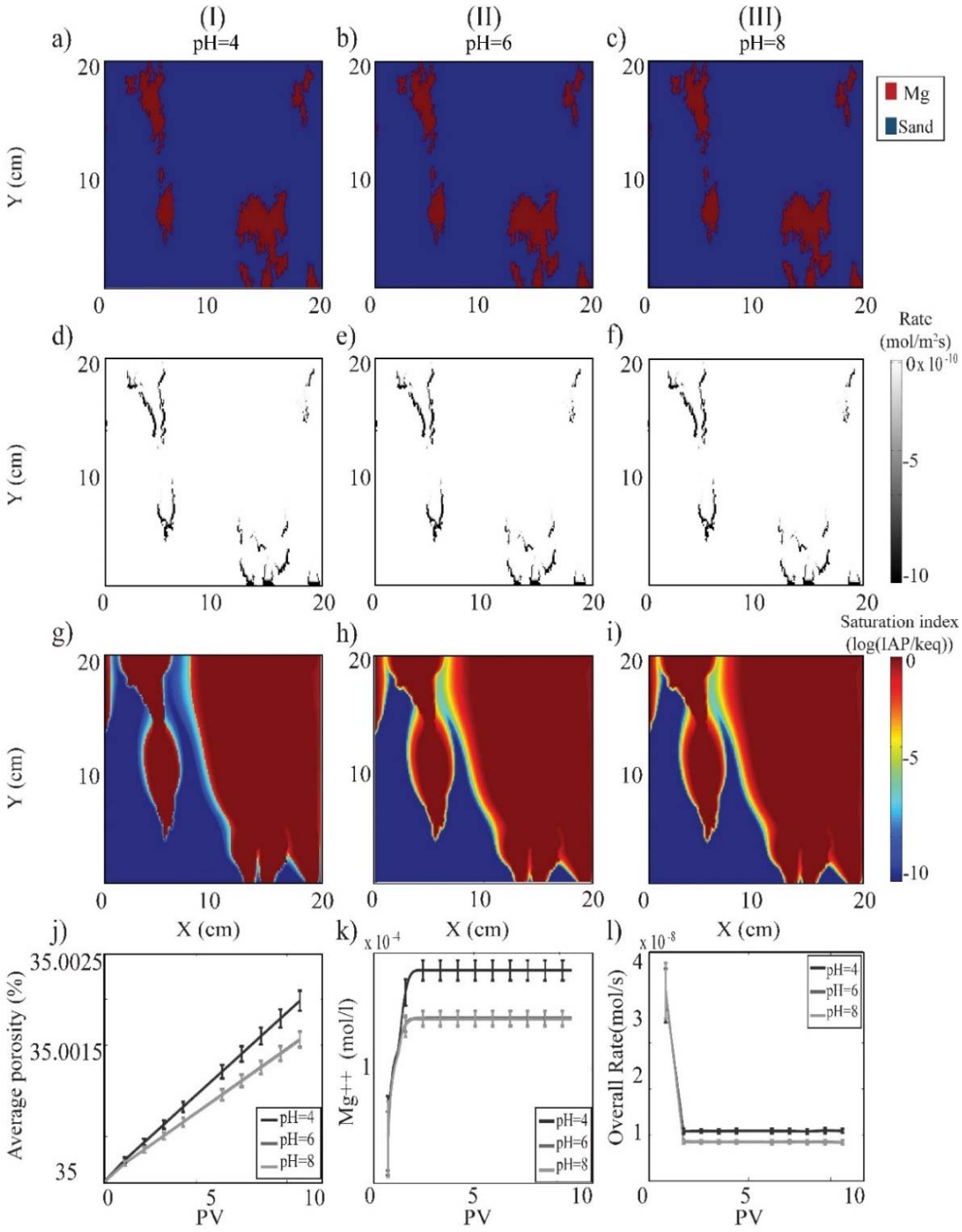


Figure 7. 2D spatial profiles of dissolution under various inlet pH (4.0, 6.0, 8.0): (a)-(d) the spatial distribution of minerals (e)-(h) spatial distribution of magnesite dissolution rate, (i)-(l) saturation index of pore solution. j) average porosity, k) concentration of Mg2+. l) overall rate of dissolution of magnesite.

After transformation, the variables in all three datasets (training, validation, and test) were standardized using the training dataset. We used the lassoCV (cross validation code) function from Python's Scikit-learn package to perform feature selection. The code used the data to determine the L1 penalty coefficient, $\lambda$ in addition to coefficients for linear regression. The most significant variables and their coefficients are presented in Table 3, with $\lambda$ =1.838e-07.

After feature selection, simple linear regression was performed to provide a base-line to compare the deep learning results. The metric used for comparison was $R^2$. The $R^2$ score for linear regression on the training dataset was 0.735. To provide a more realistic estimate of accuracy each model need to be verified using the test dataset (never used during training), which resulted in an $R^2$ score 0.732, meaning that 73.2% of the variance in the data can be accounted for using regression.

Table 3. Coefficients calculated from regression analysis

| Variable | lasso coefficients | regression coefficients |
|---|---|---|
| **Major Anisotropy** | -8.19E-05 | -5.19E-05 |
| **10 $^{\text{Major Anisotropy}}$** | -1.19E-05 | -1.51E-05 |
| **1/Major Anisotropy** | -1.19E-05 | -1.74E-05 |
| **Major Anisotropy $^{0.5}$** | -1.93E-05 | -5.42E-05 |
| **Minor Anisotropy $^{4}$** | -1.49E-05 | -1.58E-05 |
| **10 $^{\text{Minor Anisotropy}}$** | 6.68E-06 | 8.36E-06 |
| **1/Minor Anisotropy** | 1.36E-05 | 1.39E-05 |
| **log10(Minor Anisotropy)** | -4.13E-05 | -3.95E-05 |

Table 3. Coefficients calculated from regression analysis (Cont.)

| | | |
|---|---|---|
| **$10^{pH}$** | 2.62E-05 | 2.95E-05 |
| **log10(pH)** | -0.000222228 | -0.000226992 |
| **Magnesite Percentage $^{4}$** | -1.90E-05 | -2.21E-05 |
| **1/Magnesite Percentage** | -9.80E-05 | -8.06E-05 |
| **log10(Magnesite Percentage)** | 8.44E-05 | 0.000105618 |
| **$10^{Magnesite\ permeability}$** | -0.054625685 | -4326057872 |
| **$10^{-Magnesite\ permeability}$** | 0.000272208 | 8439208352 |
| **1/Magnesite permeability** | -0.054659091 | -7958133105 |
| **log10(Magnesite permeability)** | 2.39E-17 | 6432564228 |
| **Mg Perm ln(x)** | 1.96E-13 | -649160879.6 |
| **K ratio** | 0.000126931 | -1511267287 |
| **K ratio $^{0.5}$** | 0.000169472 | 539809902.4 |

## 3.7. DEEP LEARNING

As explained in the methodology section, the neural network used in this study is a deep network with 14 hidden layers. 10 linearly activated layers, followed by two tanh layers and two sigmoid layers. The output layer is only one node that gets bits of information from the last hidden sigmoid layer (Figure 1). We used the Adaptive Moment Estimation (Adam) optimization (Kingma and Ba, 2014; Ngiam et al., 2011; Sutskever et al., 2013) method to minimize the sum squared differences loss function. The weight for all connections between nodes was randomly initialized around 0 with standard deviation

of 1 (Srivastava et al., 2015; Sussillo and Abbott, 2014).The best results were obtained after learning using the whole training datasets for 5000 epochs.

The training $R^2$ score of 0.924 was achieved on several configurations using deep learning, The $R^2$ score of the validation dataset was used to choose the best architecture for testing. The validation $R^2$ score 0.888 was the highest. To provide a more realistic approximation of the accuracy of the network, the model was examined using the test dataset and $R^2$ score of 0.890 was recorded. To better understand the extent of improvements of using deep learning instead of linear regression the differences between actual porosity changes and machine learning predictions are plotted for all cases in the test dataset in Figure 8. The extent of blackness of each sub-figure in Figure 8 is an indication of the errors made by the model. A perfect model with $R^2$ score 1.0 will result in a white figure. Figure 8 (b) is much whiter compared to Figure 8 (a), which visually confirms the difference between the $R^2$ scores. It can be concluded that deep learning can better predict porosity change given the data, especially in the higher ranges of the porosity change interval.

## 4. DISCUSSION AND CONCLUSION

This work investigates the effect of physical and chemical heterogeneity on dissolution rate of magnesite. Porous media were generated using statistical parameters that represent the spatial distribution of mineral. Magnesite dissolution was simulated using CrunchFlow under various hydrogeochemical conditions. The simulations were performed under different permeability ratios (magnesite permeability/sand permeability) and inlet pH.

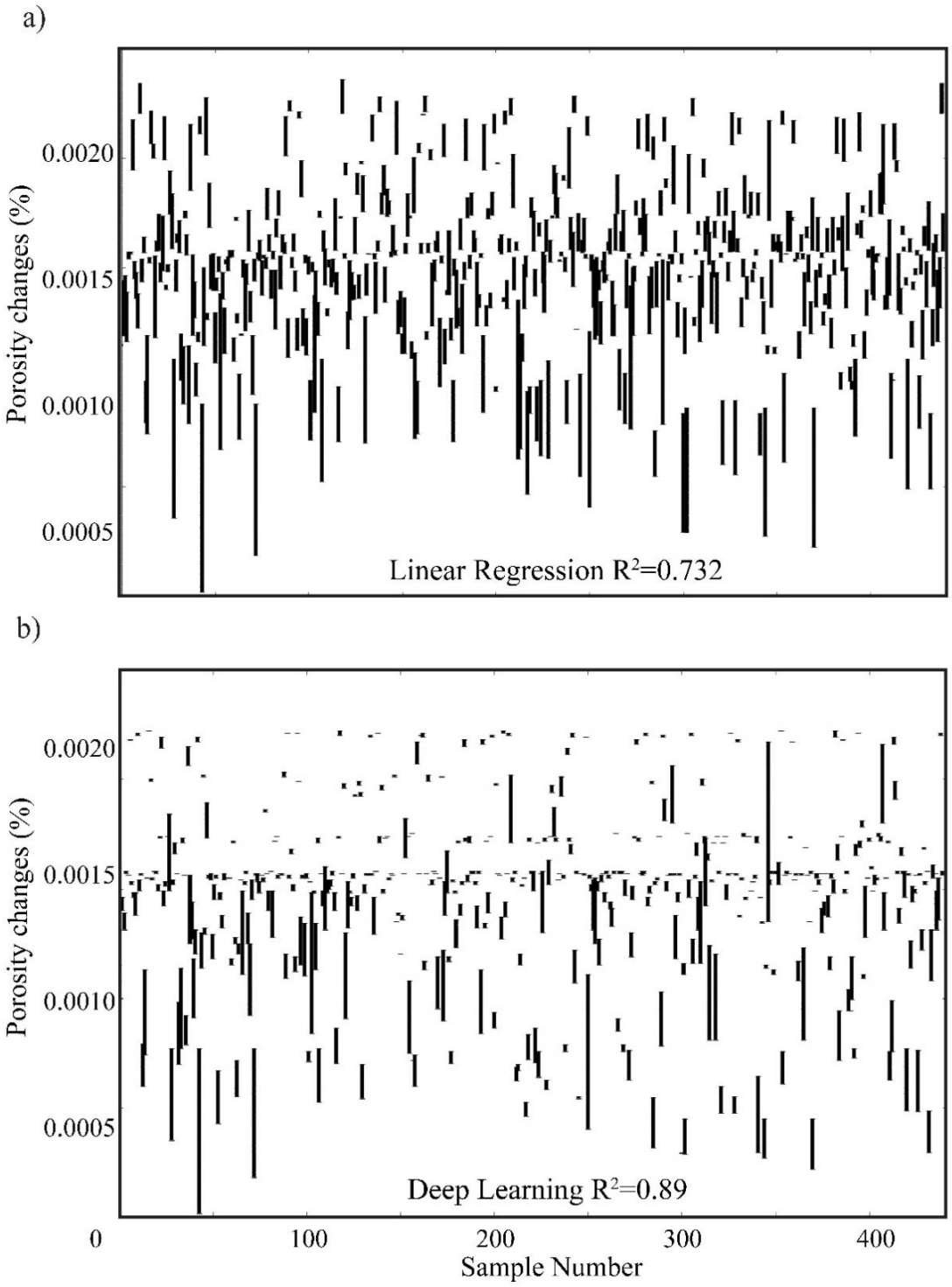


Figure 8. Differences between actual and machine learning prediction of porosity change (reaction rate) using a) linear regression and b) deep learning for all test cases. The extent of blackness of a figure is representative of the error of the method.

A total of **3257** simulations were carvarried out. Each simulation took 2-12 hours to complete. The highest change in porosity was calculated under 50% magnesite abundance at 0.0023%. The lowest porosity change was 0.0011, which occurred under a permeability ratio of 0.1. Increasing magnesite percentage by 4% resulted in 15% increase in changes of porosity. To compare on a similar scale, a 4% increase in major direction anisotropy reduced the changes of porosity by 19%. However, the same amount of change in minor direction anisotropy barely decreased the porosity changes. Increasing the permeability ratio of the reactive zone to the non-reactive zone by 99 % resulted in an 81% increase in changes of porosity. Under pH conditions of 6 and 8, porosity change was 0.0016, which is 25% less than pH 4. Permeability ratio had the most significant impact on porosity changes followed by major direction anisotropy and inlet pH.

Breakthrough concentration of $Mg^{2+}$ is closely related to porosity change. Similarly, the highest $Mg^{2+}$ concentration at steady state was $1.96 \times 10^{-4}$ (mol/l) which was obtained when the porous media consisted of 50% magnesite and the lowest concentration of $Mg^{2+}$ was $1.01 \times 10^{-4}$ (mol/l), which occurred when the permeability ratio was set to 0.1. Permeability ratio had the most significant impact on concentration of $Mg^{2+}$ with increasing the permeability ratio by 99% resulted in 82% higher concentration of $Mg^{2+}$ at steady state. Increasing the pH from 6.0 to 8.0 did not change the concentration of $Mg^{2+}$ but decreasing the pH to 4.0 increased $Mg^{2+}$ by 29%.

Overall, permeability ratio had the most significant impact on dissolution rate, porosity and concentration of $Mg^{2+}$, followed by major direction anisotropy and inlet pH. As the major and minor direction anisotropies decreases, the mineral distribution becomes closer to a homogeneous distribution. A more homogeneous distribution will

result in higher breakthrough concentration of $Mg^{2+}$ and higher porosity change because dissolution is more evenly distributed throughout the porous media (Li et al., 2014). Interestingly, the minor anisotropy direction values have the least significant impact on the dissolution of magnesite and the parameters associated with it. Further studies should investigate why minor anisotropy is significantly less effective on dissolution compared to major anisotropy. Even though changing the percentage of magnesite has affects in dissolution of magnesite, it seems to be less significant than major anisotropy values. The rate of increase of magnesite dissolution with increase of magnesite abundance in our models slowed down as the abundance reached higher than 30%. This is due to saturation of the porous media with $Mg^{2+}$ and consumption of $H^{+}$ in the pore solution.

Deep learning proved to be a very powerful tool in predicting reactive transport processes in systems as complex as dissolution in heterogeneous porous media. With just using the statistical parameters that can be measure in the fields and without any interference of the underlying spatial distribution of minerals, deep learning captured 89.0 % of the variance in the data while linear regression only captured 73.2%. Our study confirms the capability of using artificial engineering and machine learning in the areas of engineering and science where the underlying physics and conditions are very complex or difficult to measure.

## REFERENCES

Alekseyev, V.A., Medvedeva, L.S., Prisyagina, N.I., Meshalkin, S.S., Balabin, A.I., 1997. Change in the dissolution rates of alkali feldspars as a result of secondary mineral precipitation and approach to equilibrium. Geochim. Cosmochim. Acta 61, 1125-1142.

Allen-King, R.M., Halket, R.M., Gaylord, D.R., Robin, M.J.L., 1998. Characterizing the heterogeneity and correlation of perchloroethene sorption and hydraulic conductivity using a facies-based approach. Water Resources Research 34, 385-396.

Almasri, M.N., Kaluarachchi, J.J., 2005. Modular neural networks to predict the nitrate distribution in ground water using the on-ground nitrogen loading and recharge data. Environmental Modelling & Software 20, 851-871.

Anbeek, C., 1993. THE EFFECT OF NATURAL WEATHERING ON DISSOLUTION RATES. Geochimica Et Cosmochimica Acta 57, 4963-4975.

Barber, L.B., Thurman, E.M., Runnells, D.D., 1992. GEOCHEMICAL HETEROGENEITY IN A SAND AND GRAVEL AQUIFER - EFFECT OF SEDIMENT MINERALOGY AND PARTICLE-SIZE ON THE SORPTION OF CHLOROBENZENES. Journal of Contaminant Hydrology 9, 35-54.

Bengio, Y., 2009. Learning deep architectures for AI. Foundations and trends® in Machine Learning 2, 1-127.

Berner, 1981. Early diagnostic : A theoretical approach. Eos, Transactions American Geophysical Union 62, 510-511.

Berner, R.A., 1995. Chemical weathering and its effect on atmospheric CO2 and climate. Chemical Weathering Rates of Silicate Minerals 31, 565-583.

Birkefeld, A., Schulin, R., Nowack, B., 2006. In situ investigation of dissolution of heavy metal containing mineral particles in an acidic forest soil. Geochim. Cosmochim. Acta 70, 2726-2736.

Boggs, J.M., Young, S.C., Beard, L.M., Gelhar, L.W., Rehfeldt, K.R., Adams, E.E., 1992. FIELD-STUDY OF DISPERSION IN A HETEROGENEOUS AQUIFER .1. OVERVIEW AND SITE DESCRIPTION. Water Resources Research 28, 3281-3291.

Bohling, G., 2005. Introduction to geostatistics and variogram analysis. Kansas geological survey, 20p.

Brantley, S.L., White, A.F., 2009. Approaches to Modeling Weathered Regolith, in: Oelkers, E.H., Schott, J. (Eds.), Thermodynamics and Kinetics of Water-Rock Interaction, pp. 435-484.

Chou, L., Garrels, R.M., Wollast, R., 1989. Comparative study of the kinetics and mechanisms of dissolution of carbonate minerals. Chemical Geology 78, 269-282.

Coppola, E., Szidarovszky, F., Poulton, M., Charles, E., 2003. Artificial neural network approach for predicting transient water levels in a multilayered groundwater system under variable state, pumping, and climate conditions. J. Hydrol. Eng. 8, 348-360.

De Windt, L., Pellegrini, D., van der Lee, J., 2004. Reactive transport modelling of a spent fuel repository in a stiff clay formation considering excavation damaged zones. Radiochimica Acta 92, 841-848.

Deng, L., Yu, D., 2014. Deep Learning. Signal Processing 7, 3-4.

Dentz, M., Gouze, P., Carrera, J., 2011a. Effective non-local reaction kinetics for transport in physically and chemically heterogeneous media. Journal of Contaminant Hydrology 120-21, 222-236.

Dentz, M., Le Borgne, T., Englert, A., Bijeljic, B., 2011b. Mixing, spreading and reaction in heterogeneous media: A brief review. Journal of Contaminant Hydrology 120-21, 1-17.

Espinoza, C., Valocchi, A.J., 1998. TEMPORAL MOMENTS ANALYSIS OF TRANSPORT IN CHEMICALLY HETEROGENEOUS POROUS MEDIA. J. Hydrol. Eng. 3, 276-284.

Frank, I.E., Friedman, J.H., 1993. A STATISTICAL VIEW OF SOME CHEMOMETRICS REGRESSION TOOLS. Technometrics 35, 109-135.

Gaur, S., Ch, S., Graillot, D., Chahar, B.R., Kumar, D.N., 2013. Application of Artificial Neural Networks and Particle Swarm Optimization for the Management of Groundwater Resources. Water Resources Management 27, 927-941.

Gringarten, E., Deutsch, C.V., 2001. Teacher's Aide Variogram Interpretation and Modeling. Mathematical Geology 33, 507-534.

Gümrah, F., Öz, B., Güler, B., Evin, S., 2000. The application of artificial neural networks for the prediction of water quality of polluted aquifer. Water, Air, and Soil Pollution 119, 275-294.

Guruprasad, B., Indraratna, B., Nghiem, L.D., Regmi, G., 2011. A neural network approach to predict the performance of recycled concrete used in permeable reactive barriers for the treatment of acidic groundwater. Quarterly Journal of Engineering Geology and Hydrogeology 44, 199-209.

Hastie, T., Tibshirani, R. and Friedman, J., 2009. Elements of Statistical Learning: Data Mining, Inference and Prediction. New York: Springer 2nd edn.

Heidari, P., 2014. Effects of physical and chemical heterogeneities on transport and reaction processes in porous media. PhD dissertation, Pennsylvania State University.

Heidari, P., Li, L., 2014. Solute transport in low-heterogeneity sand boxes: The role of correlation length and permeability variance. Water Resources Research 50, 8240-8264.

Hinton, G.E., Osindero, S., Teh, Y.W., 2006. A fast learning algorithm for deep belief nets. Neural Comput. 18, 1527-1554.

Hoerl, A.E., Kennard, R.W., 2004. Ridge Regression, Encyclopedia of Statistical Sciences. John Wiley & Sons, Inc.

Huntington, T.G., 2000. The potential for calcium depletion in forest ecosystems of southeastern United States: Review and analysis. Global Biogeochemical Cycles 14, 623-638.

Jahreis, K., 2015. Measurement Error in LASSO-Analytical Results and a Simulation Study.

Kingma, D., Ba, J., 2014. Adam: A method for stochastic optimization. arXiv preprint arXiv:1412.6980.

LeCun, Y., Bengio, Y., Hinton, G., 2015. Deep learning. Nature 521, 436-444.

Li, L., Gawande, N., Kowalsky, M.B., Steefel, C.I., Hubbard, S.S., 2011. Physicochemical Heterogeneity Controls on Uranium Bioreduction Rates at the Field Scale. Environ. Sci. Technol. 45, 9959-9966.

Li, L., Peters, C.A., Celia, M.A., 2006. Upscaling geochemical reaction rates using pore-scale network modeling. Adv. Water Resour. 29, 1351-1370.

Li, L., Peters, C.A., Celia, M.A., 2007a. Effects of mineral spatial distribution on reaction rates in porous media. Water Resources Research 43, 17.

Li, L., Peters, C.A., Celia, M.A., 2007b. Effects of mineral spatial distribution on reaction rates in porous media. Water Resources Research 43, 1-17.

Li, L., Salehikhoo, F., Brantley, S.L., Heidari, P., 2014. Spatial zonation limits magnesite dissolution in porous media. Geochim. Cosmochim. Acta 126, 555-573.

Liermann, L.J., Mathur, R., Wasylenki, L.E., Nuester, J., Anbar, A.D., Brantley, S.L., 2011. Extent and isotopic composition of Fe and Mo release from two Pennsylvania shales in the presence of organic ligands and bacteria. Chemical Geology 281, 167-180.

Lischeid, G., Buttcher, H., Hauck, A., 2003. Combining data-based and process-based approaches to minimize the complexity of a reactive sulphate transport model, in: Kovar, K., Hrkal, Z. (Eds.), Calibration and Reliability in Groundwater Modelling: A Few Steps Closer to Reality. Int Assoc Hydrological Sciences, Wallingford, pp. 402-408.

Luciano, A., Viotti, P., Torretta, V., Mancini, G., 2013. Numerical approach to modelling pulse-mode soil flushing on a Pb-contaminated soil. J. Soils Sediments 13, 43-55.

Maher, K., DePaolo, D.J., Lin, J.C.F., 2004. Rates of silicate dissolution in deep-sea sediment: In situ measurement using U-234/U-238 of pore fluids. Geochimica Et Cosmochimica Acta 68, 4629-4648.

Maher, K., Steefel, C.I., DePaolo, D.J., Viani, B.E., 2006. The mineral dissolution rate conundrum: Insights from reactive transport modeling of U isotopes and pore fluid chemistry in marine sediments. Geochimica Et Cosmochimica Acta 70, 337-363.

Maher, K., Steefel, C.I., White, A.F., Stonestrom, D.A., 2009. The role of reaction affinity and secondary minerals in regulating chemical weathering rates at the Santa Cruz Soil Chronosequence, California. Geochim. Cosmochim. Acta 73, 2804-2831.

Maier, H.R., Dandy, G.C., 1998. Understanding the behaviour and optimising the performance of back-propagation neural networks: An empirical study. Environmental Modelling and Software 13, 179-191.

Manto, H., 2005. Modelling of geometric anisotropic spatial variation. Mathematical Modelling and Analysis, 361-366.

Mayer, A.S., Kelley, C.T., Miller, C.T., 2002. Optimal design for problems involving flow and transport phenomena in saturated subsurface systems. Adv. Water Resour. 25, 1233-1256.

McCulloch, W.S., Pitts, W., 1943. A logical calculus of the ideas immanent in nervous activity. The Bulletin of Mathematical Biophysics 5, 115-133.

Meile, C., Tuncay, K., 2006. Scale dependence of reaction rates in porous media. Adv. Water Resour. 29, 62-71.

Meinshausen, N., Bühlmann, P., 2006. High-dimensional graphs and variable selection with the lasso. The annals of statistics, 1436-1462.

Molins, S., Trebotich, D., Steefel, C.I., Shen, C., 2012. An investigation of the effect of pore scale flow on average geochemical reaction rates using direct numerical simulation. Water Resources Research 48, n/a-n/a.

Moore, J., Lichtner, P.C., White, A.F., Brantley, S.L., 2012. Using a reactive transport model to elucidate differences between laboratory and field dissolution rates in regolith. Geochimica Et Cosmochimica Acta 93, 235-261.

Morrison, S.J., Goodknight, C.S., Tigar, A.D., Bush, R.P., Gil, A., 2012. Naturally Occurring Contamination in the Mancos Shale. Environmental Science & Technology 46, 1379-1387.

Morshed, J., Kaluarachchi, J.J., 1998a. Application of artificial neural network and genetic algorithm in flow and transport simulations. Adv. Water Resour. 22, 145-158.

Morshed, J., Kaluarachchi, J.J., 1998b. Parameter estimation using artificial neural network and genetic algorithm for free-product migration and recovery. Water Resources Research 34, 1101-1113.

Navarre-Sitchler, A., Brantley, S., 2007. Basalt weathering across scales. Earth Planet. Sci. Lett. 261, 321-334.

Ngiam, J., Coates, A., Lahiri, A., Prochnow, B., Le, Q.V., Ng, A.Y., 2011. On optimization methods for deep learning, Proceedings of the 28th International Conference on Machine Learning (ICML-11), pp. 265-272.

Nikolos, I.K., Stergiadi, M., Papadopoulou, M.P., Karatzas, G.P., 2008. Artificial neural networks as an alternative approach to groundwater numerical modelling and environmental design. Hydrological Processes 22, 3337-3348.

Piotrowski, A.P., Napiorkowski, J.J., Osuch, M., Napiorkowski, M.J., 2016. On the importance of training methods and ensemble aggregation for runoff prediction by means of artificial neural networks. Hydrological Sciences Journal-Journal Des Sciences Hydrologiques 61, 1903-1925.

Plummer, L., Wigley, T., Parkhurst, D., 1978. The kinetics of calcite dissolution in CO 2-water systems at 5 degrees to 60 degrees C and 0.0 to 1.0 atm CO 2. American Journal of Science 278, 179-216.

Pokrovsky, O.S., Golubev, S.V., Schott, J., Castillo, A., 2009. Calcite, dolomite and magnesite dissolution kinetics in aqueous solutions at acid to circumneutral pH, 25 to 150 degrees C and 1 to 55 atm pCO(2): New constraints on CO2 sequestration in sedimentary basins. Chemical Geology 265, 20-32.

Pokrovsky, O.S., Schott, J., 1999. Processes at the magnesium-bearing carbonates solution interface. II. Kinetics and mechanism of magnesite dissolution. Geochim. Cosmochim. Acta 63, 881-897.

Reeves, D., Rothman, D.H., 2013. Age dependence of mineral dissolution and precipitation rates. Global Biogeochemical Cycles 27, 906-919.

Renard, P., Allard, D., 2013. Connectivity metrics for subsurface flow and transport. Adv. Water Resour. 51, 168-196.

Rizzo, D.M., Dougherty, D.E., 1994. Characterization of aquifer properties using artificial neural networks: Neural kriging. Water Resources Research 30, 483-497.

Rizzo, D.M., Dougherty, D.E., 1996. Design Optimization for Multiple Management Period Groundwater Remediation. Water Resources Research 32, 2549-2561.

Rogers, L.L., Dowla, F.U., 1994. Optimization of groundwater remediation using artificial neural networks with parallel solute transport modeling. Water Resources Research 30, 457-481.

Rumelhart, D., 1986. Parallel distributed processing: explorations in the microstructure of cognition, vol. 1: foundations, in: David, E.R., James, L.M., Group, C.P.R. (Eds.). MIT Press, p. 547.

Salehikhoo, F., Li, L., 2015. The role of magnesite spatial distribution patterns in determining dissolution rates: When do they matter? Geochim. Cosmochim. Acta 155, 107-121.

Salehikhoo, F., Li, L., Brantley, S.L., 2013. Magnesite dissolution rates at different spatial scales: The role of mineral spatial distribution and flow velocity. Geochimica Et Cosmochimica Acta 108, 91-106.

Schmidhuber, J., 2015. Deep learning in neural networks: An overview. Neural Netw. 61, 85-117.

Singha, K., Li, L., Day-Lewis, F.D., Regberg, A.B., 2011. Quantifying solute transport processes: Are chemically "conservative" tracers electrically conservative? Geophysics 76, F53-F63.

Smith, M.M., Sholokhova, Y., Hao, Y., Carroll, S.A., 2013. CO2-induced dissolution of low permeability carbonates. Part I: Characterization and experiments. Advances in Water Resources 62, 370-387.

Sobanska, S., Ledesert, B., Deneele, D., Laboudigue, A., 2000. Alteration in soils of slag particles resulting from lead smelting. Comptes Rendus De L Academie Des Sciences Serie Ii Fascicule a-Sciences De La Terre Et Des Planetes 331, 271-278.

Song, X.D., Zhang, G.L., Liu, F., Li, D.C., Zhao, Y.G., Yang, J.L., 2016. Modeling spatio-temporal distribution of soil moisture by deep learning-based cellular automata model. Journal of Arid Land 8, 734-748.

Srivastava, R.K., Greff, K., Schmidhuber, J., 2015. Training very deep networks, Advances in neural information processing systems, pp. 2377-2385.

Steefel, C., 2009. Fluid-rock interaction: A reactive transport approach.

Steefel, C.I., Carroll, S., Zhao, P.H., Roberts, S., 2003. Cesium migration in Hanford sediment: a multisite cation exchange model based on laboratory transport experiments. Journal of Contaminant Hydrology 67, 219-246.

Steefel, C.I., Lichtner, P.C., 1994. Diffusion and reaction in rock matrix bordering a hyperalkaline fluid-filled fracture. Geochim. Cosmochim. Acta 58, 3595-3612.

Steefel, C.I., Vancappellen, P., 1990. A NEW KINETIC APPROACH TO MODELING WATER-ROCK INTERACTION - THE ROLE OF NUCLEATION, PRECURSORS, AND OSTWALD RIPENING. Geochimica Et Cosmochimica Acta 54, 2657-2677.

Sudicky, E.A., Illman, W.A., Goltz, I.K., Adams, J.J., McLaren, R.G., 2010. Heterogeneity in hydraulic conductivity and its role on the macroscale transport of a solute plume: From measurements to a practical application of stochastic flow and transport theory. Water Resources Research 46, 1-16.

Sussillo, D., Abbott, L., 2014. Random walk initialization for training very deep feedforward networks. arXiv preprint arXiv:1412.6558.

Sutskever, I., Martens, J., Dahl, G.E., Hinton, G.E., 2013. On the importance of initialization and momentum in deep learning. ICML (3) 28, 1139-1147.

Tibshirani, R., 1996. Regression shrinkage and selection via the Lasso. J. R. Stat. Soc. Ser. B-Methodol. 58, 267-288.

Tompson, A.F.B., Jackson, K.J., 1996. Reactive transport in heterogeneous systems: An overview, in: Lichtner, P.C., Steefel, C.I., Oelkers, E.H. (Eds.), Reactive Transport in Porous Media, pp. 269-310.

Tsai, W.P., Chiang, Y.M., Huang, J.L., Chang, F.J., 2016. Exploring the Mechanism of Surface and Ground Water through Data-Driven Techniques with Sensitivity Analysis for Water Resources Management. Water Resources Management 30, 4789-4806.

van der Lee, J., De Windt, L., 2001. Present state and future directions of modeling of geochemistry in hydrogeological systems. Journal of Contaminant Hydrology 47, 265-282.

Warrick, A., Myers, D., 1987. Optimization of sampling locations for variogram calculations. Water Resources Research 23, 496-500.

Webster, R., Oliver, M.A., 1993. How large a sample is needed to estimate the regional variogram adequately?, in: Soares, A. (Ed.), Geostatistics Tróia '92: Volume 1. Springer Netherlands, Dordrecht, pp. 155-166.

White, A.F., Brantley, S.L., 2003. The effect of time on the weathering of silicate minerals: why do weathering rates differ in the laboratory and field? Chemical Geology 202, 479-506.

White, A.F., Schulz, M.S., Vivit, D.V., Blum, A.E., Stonestrom, D.A., Harden, J.W., 2005. Chemical weathering rates of a soil chronosequence on granitic alluvium: III. Hydrochemical evolution and contemporary solute fluxes and rates. Geochimica Et Cosmochimica Acta 69, 1975-1996.

Willmann, M., Carrera, J., Sanchez-Vila, X., 2008. Transport upscaling in heterogeneous aquifers: What physical parameters control memory functions? Water Resources Research 44, 1-13.

Wolery, T.J., Jackson, K.J., Bourcier, W.L., Bruton, C.J., Viani, B.E., Knauss, K.G., Delany, J.M., 1990. CURRENT STATUS OF THE EQ3/6 SOFTWARE PACKAGE FOR GEOCHEMICAL MODELING.

Xu, T.F., White, S.P., Pruess, K., Brimhall, G.H., 2000. Modeling of pyrite oxidation in saturated and unsaturated subsurface flow systems. Transport in Porous Media 39, 25-56.

Yan, S., Minsker, B., 2006. Optimal groundwater remediation design using an Adaptive Neural Network Genetic Algorithm. Water Resources Research 42, n/a-n/a.

Yokoyama, S., Kuroda, M., Sato, T., 2005. Atomic force microscopy study of montmorillonite dissolution under highly alkaline conditions. Clay Clay Min. 53, 147-154.

Zhao, P., Yu, B., 2006. On model selection consistency of Lasso. Journal of Machine Learning Research 7, 2541-2563.

Zhu, J.F., Cai, X., Yeh, T.C.J., 2009. Analysis of tracer tomography using temporal moments of tracer breakthrough curves. Advances in Water Resources 32, 391-400.

Zinn, B., Harvey, C.F., 2003. When good statistical models of aquifer heterogeneity go bad: A comparison of flow, dispersion, and mass transfer in connected and multivariate Gaussian hydraulic conductivity fields. Water Resources Research 39, 1-19.

Zou, H., 2006. The adaptive lasso and its oracle properties. Journal of the American statistical association 101, 1418-1429.

Zou, H., Hastie, T., 2005. Regularization and variable selection via the elastic net. Journal of the Royal Statistical Society: Series B (Statistical Methodology) 67, 301-320.

# II. DATA-DRIVEN STUDY OF NON-REACTIVE CONTAMINANT ATTENUATION TIME IN HETEROGENOUS POROUS MEDIA

Mahta Gholizadeh Ansari[1], Peyman Heidari[1,*]

[1] Missouri University of Science and Technology, Department of Geosciences and Geological and Petroleum Engineering.

## ABSTRACT

This work examines how heterogeneity can affect solute transport and attenuation time in porous media. Different spatial distributions were created by using statistical parameters such as different permeability standard deviation, as well as major and minor direction anisotropies. The solute transport was simulated under various flow rates and transverse dispersivity values. A total of **3536** simulations were carried out in CrunchFlow. Standard deviation proved to have the most significant impact on attenuation time, followed by major and minor direction anisotropies. A more heterogeneous and anisotropic distribution resulted in a time delay in concentration reduction. The effect of anisotropies were trivial in a relatively homogenous distribution. On the contrary, the effect of transverse dispersivity was only significant when heterogeneity was low. Lasso regression was used for feature selection and a linear regression model was created based on the selected features. The linear model can describe 70.83 % of the variance in the data.

# 1. INTRODUCTION

Ground water contamination is known to be one of the most important environmental concerns in recent years (Wang and Huang, 2011). Quantifying flow and predicting contaminant transport are essential in many fields such as groundwater hydrology (remediation and quality improvement), waste disposal and subsurface CO2 storage (Gjetvaj et al., 2015; Gouze et al., 2008; Wang and Huang, 2011; Yoon et al., 2015). The heterogeneity of natural subsurface and insufficient data make it difficult to estimate the hydraulic variables and subsequently an accurate estimation of flow and transport in natural subsurface will be difficult to attain (Wang and Huang, 2011). Solute transport in natural subsurface depends on chemical, microbial and physical processes. The transport of a solute is a combination of various processes, such as convective transport, dispersion, molecular diffusion and in cases where reactive species are involved, production, decay and equilibrium or non-equilibrium exchange with solid phase (SHARMA and ABGAZE, 2015). Solute transport in heterogeneous media has been studied in experimental (Chao et al., 2000; Cortis and Berkowitz, 2004; Levy and Berkowitz, 2003; Silliman, 2001), numerical (Brusseau et al., 1989; Fernandez-Garcia et al., 2005; Goltz and Roberts, 1986; Valocchi, 1985; Willmann et al., 2008) and field research (Adams and Gelhar, 1992; Garabedian et al., 1991; Welty and Gelhar, 1994).

The Advection Dispersion Equation (ADE) works well under the assumption that Fick's first law applies well to tracer transport in homogenous media (Berkowitz et al., 2006; Zhang et al., 2016). However, transport in the heterogeneous system has been established as non-Fickan and therefore cannot be accurately modeled by the ADE (Berkowitz et al., 2006). In order to quantify the anolomous and non Fickian behavior

different models have been proposed such as multi rate mass transfer model (Haggerty and Gorelick, 1995), dual porosity model (Gerke and Vangenuchten, 1993), Continuous Time Random Walk which has non-locality in time (Berkowitz and Scher, 1998, 2001; Berkowitz et al., 2000) and Fractional Advection Dispersion Equation which is spatially non local (Benson et al., 2000a, b; Meerschaert Mark and Sikorskii, 2011; Meerschaert et al., 1999; Zhang et al., 2016).

Various spatial patterns can be observed in natural subsurface due to the uneven distribution of solid material (Allen-King et al., 1998; Barber et al., 1992; de Marsily et al., 2005; Scheibe et al., 2011; Sudicky et al., 2010a; Zinn and Harvey, 2003). The mineral distribution in the porous media, which can vary from patches to layers, causes spatial variation in the subsurface and significantly changes its flow and transport properties (Bao et al., 2014; Jin et al., 2013; Landrot et al., 2012; Li et al., 2011; Nicolaides et al., 2015). The impacts of permeability variations on macrodispersion and spreading tracers have been studied over the past few decades (Berkowitz et al., 2006; Dagan, 1990, 2004; Dagan et al., 2013; Dentz et al., 2004; Zhang and Neuman, 1990).

The quantification of effective permeability in most studies involves mathematical, geostatistical, numerical and stochastic methods with synthetic or imaged small scale distribution (Babadagli, 2006; Desbarats and Bachu, 1994; Di Federico et al., 2010; Sun et al., 2011; Vernerey, 2012). The effective permeability is highly dependent to pore connectivity, ratio of high permeability zones to the entire media and the direction of the mineral distribution and the flow (Bernabe et al., 2003; Bernabe et al., 2004; Bernabe et al., 2011). Effective permeability depends on both spatial distribution characteristics and magnitude of permeability variations (Desbarats and Bachu, 1994).

Effective permeability is derived from the arithmetic average of layers parallel to the flow and the harmonic average of layers perpendicular to the flow (Song and Renner, 2006).

It is widely known that proper understanding of the heterogeneity and the spatial distribution of a system is crucial for estimation and prediction of solute transport (de Dreuzy and Davy, 2007; Heidari and Li, 2014b; Jankovic et al., 2003; Pedretti et al., 2013; Pedretti et al., 2016; Ramasomanana et al., 2013).Moreover, Connectivity and correlation length has been recognized by numerous studies as main parameters in solute breakthrough (Renard and Allard, 2013; Willmann et al., 2008). Dispersivity increases as the connectivity in relatively low conductivity layers increases (Zinn et al., 2004). Moreover, with the incline in connectivity of the low conductivity layers the breakthrough curves tailing increases (Willmann et al., 2008). According to Pedertti (2013) the shape of the breakthrough curves can be altered by permeability variation in vertical layers.

Several studies demonstrated that permeability has high spatial variation, meaning that its maximum value can be larger than its minimum value by several orders of magnitude, while the variation in other parameters remain relatively minor (Gelhar, 1986; Russo and Bouton, 1992; Zhang and Neuman, 1990). Most of previous solute transport modeling studies had limited permeability variation, the goal of this study is to quantify and predict the transport of non-reactive contaminant in heterogeneous non-reactive porous media with high variation in permeability values, using a modeling approach.

# 2. METHODOLOGY

## 2.1. POROUS MEDIA DESCRIPTION

The goal of this study is to investigate the effects of physical heterogeneity on the attenuation time of non-reactive contaminants. The dimensions of the quasi-2D porous medium is 200mm×200mm×1mm. The modeling domain has 40,000 grid blocks of 1mm×1mm×1mm which consist of sand zones with variable permeability. Spatial distributions of permeability were created in porous media using PETREL. PETREL can create replicas of different porous media which can be of use when interpreting seismic data, and performing well correlation, which is normally used in the oil and gas industry (Gringarten and Deutsch, 2001). In order to create a 2D realization of the porous medium, major and minor direction anisotropies, a variogram model, mean and standard deviation are inserted in the software.

Variograms are widely used in geostatistical analysis to describe the spatial relationship between values of a parameter (Webster and Oliver, 1993). The variogram equation is (Gringarten and Deutsch, 2001; Warrick and Myers, 1987):

$$2\gamma(\mathrm{h}) = \mathrm{E}[\mathrm{Y}(\mathrm{u}) - \mathrm{Y}(\mathrm{u}+\mathrm{h})]^2 \qquad (6)$$

where *Y* represents a stationary random function and $h$ stands for a distance vector. In other words, the variogram defines the expected square difference for different data with a distance vector of *h* (Gringarten and Deutsch, 2001). A semivariogram $\gamma(h)$, which is half of the variogram, $2\gamma(h)$ , is described by sill, range and nugget. The non-zero value of a semivariogram at its origin is called a nugget, which also can represent the measurement error (Bohling, 2005; Gringarten and Deutsch, 2001; Manto, 2005). The sill ( $\gamma_\infty$) value is the description of the variance of the random field without accounting

for the spatial structure (Gringarten and Deutsch, 2001; Manto, 2005). Range or anisotropy is the distance at which sill is reached by the semivariogram (Bohling, 2005). In this study the values for the nugget and sill are 0.0001 and 1.0, respectively.

The most commonly studied variogram models are those with a sill, such as a spherical model, exponential model, Gaussian model or nugget model (Bohling, 2005; Gringarten and Deutsch, 2001; Warrick and Myers, 1987). An anisotropic variogram is defined as a semivariogram that its values change with direction (Manto, 2005). Numerous studies report that permeability has a lognormal distribution (Garabedian et al., 1991; Jankovic et al., 2003; Renard and deMarsily, 1997; Sudicky et al., 2010b; Wang and Huang, 2011). Thus, a lognormal model was chosen for the anisotropic variogram.

In this study, the mean value of 17576 milidarcy and the standard deviation of 11232 md were derived from Botany aquifer study (Jankowski and Beck, 2000). In order to better understand the impact of permeability variations four sets of standard deviation values of 11.232, 112.32, 1123.2 and 11232 were inserted in PETREL. Fourteen different pairs of major and minor direction anisotropies were chosen for this study as shown in Table 1. After providing all required inputs, the software will randomly generate a spatial distribution. Ten different realizations were generated for each combination (for example, standard deviation=112, major direction anisotropy= 50 mm, major direction anisotropy=50 mm) to reduce the effect of any specific spatial distribution.

Table 1. Major and minor direction anisotropies

| Combination | Major(mm) | Minor(mm) | Combination | Major(mm) | Minor(mm) |
|---|---|---|---|---|---|

Table 1. Major and minor direction anisotropies (Cont.)

| | | | | | |
|---|---|---|---|---|---|
| **Case 1** | **1** | **1** | **Case 8** | **50** | **10** |
| **Case 2** | 10 | 1 | **Case 9** | 50 | 20 |
| **Case 3** | 10 | 10 | **Case 10** | 50 | 50 |
| **Case 4** | 20 | 1 | **Case 11** | 100 | 1 |
| **Case 5** | 20 | 10 | **Case 12** | 100 | 20 |
| **Case 6** | 20 | 20 | **Case 13** | 100 | 50 |
| **Case 7** | 50 | 1 | **Case 14** | 100 | 100 |

## 2.2. REACTIVE TRANSPORT MODELING

The traditional Advection Dispersion Equation (ADE) is used to quantify transport of non-reactive chemical at Darcy scale (Gjetvaj et al., 2015; Heidari and Li, 2014b). In the ADE method it is assumed that variation of advective fluxes and diffusion will create a hydrodynamic dispersion which resembles a diffusion-like (Fickian) process in the macro scale (Bear, 1988; Gjetvaj et al., 2015).

$$\frac{\partial C}{\partial t} + \nabla . (-D\nabla \mathrm{C} + \mathrm{vC}) = 0 \qquad (1)$$

C is concentration of solute (mol/l$^3$), t is time (s), D is dispersion diffusion tensor (m$^2$/s), v is the velocity vector whose basis consists of two vectors in which are parallel and perpendicular to the main flow (Heidari and Li, 2014b).The dispersion diffusion D is the sum of the effective diffusion coefficient D$^*$ (m$^2$/s) and the mechanical dispersion coefficient. In any grid block in the porous media, $v_x$ and $v_y$ are flow velocities in longitudinal and transverse direction and their corresponding dispersion coefficients ($D_L$ and $D_T$ ) can be derived from the following equations.

$$D_L = D^* + \alpha_L v_x \quad (2)$$

$$D_T = D^* + \alpha_T v_y \quad (3)$$

$\alpha_L$ and $\alpha_T$ are the longitudinal and transverse dispersivity (m). Gelhar et al. (1992) has demonstrated that the longitudinal dispersivity is usually 6 to 20 times larger than the transverse disperpersivity. In this study, diffusion was set to $10^{-5}$ $cm^2/s$.

All the numerical simulations were carried out using CrunchFlow, a pertinent code for geochemical modeling of reactive transport processes in the subsurface (Heidari and Li, 2014a; Li et al., 2011; Maher et al., 2009; Singha et al., 2011; Steefel et al., 2003; Steefel and Lichtner, 1994). The Advection Dispersion Equation (Eq (1)) was solved using the code. The initial and inlet conditions for magnesite dissolution are shown in Table 2. All simulations were performed with 35% porosity with longitudinal dispersivity of 0.05 (Heidari and Li, 2014a) and transverse dispersivity was set to 0.01, 0.001 and 0.005. In order to examine the effect of flow rate, each of the simulation sets were run with flow rate of 1, 5 and 25 (ml/min). For each of the treatment combinations mentioned above, simulations were carried out for all the unique spatial distributions obtained from PETREL, which lead to a total of **3536** simulations.

Table 2. Initial and inlet conditions

| Species | Inlet condition(mol/l) | Initial conditions(mol/l) |
|---|---|---|
| **pH** | 6.0 | 7.0 |
| **SiO2(aq)** | 1.2581E-9 | 1.0E-9 |
| **CO2(aq)** | 1.2581E-9 | 1.2581E-9 |
| **$Br^-$** | 1.2581E-9 | 1.00E-4 |

## 2.3. DATA ANALYSIS

**2.3.1. Data Transformation.** In this study, the pore volume at which concentration reaches 0.01 of the initial condition was chosen to be the dependent variable. The standard deviation, flow rate, transverse dispersivity, and major and minor direction anisotropy were the independent variables. In order to capture the possible non-linear features based on the independent variables, each variable was transformed using the following non-linear functions: $\boldsymbol{x^2}$, $\boldsymbol{x^3}$, $\boldsymbol{x^4}$, $\boldsymbol{\frac{1}{x}}$, $\boldsymbol{10^x}$, $\boldsymbol{10^{-x}}$, $\boldsymbol{log\ (x)}$, $\boldsymbol{ln(x)}$, $\boldsymbol{\sqrt[2]{x}}$, $\boldsymbol{\sqrt[3]{x}}$. Therefore, each case started with 5 features that were then turned into 55 features using the above transformation.

**2.3.2. Feature Selection.** The least absolute shrinkage and selection operator (Lasso) regression method was chosen to select the best features. Tibshirani (1996) proposed lasso regression to compensate for the short comings of subset selection and ridge regression methods.

The model selected by the subset selection is very sensitive to the slightest changes in the data which have a negative impact on the accuracy of the model (Frank and Friedman, 1993; Tibshirani, 1996). Moreover, selecting the most effective independent variable is also challenging with ridge regression, because despite the fact that it shrinks some of the coefficients (Hoerl and Kennard, 2004) it does not assign 0 to any of them (Tibshirani, 1996).

Lasso regression has been commonly used for variable selection (Meinshausen and Bühlmann, 2006; Zhao and Yu, 2006; Zou, 2006). Lasso regression imposes a penalty in the form of the absolute value of the coefficients. Lasso eases the selection by an algorithm that continuously shrinks the coefficients and assign a zero coefficient to

some of the variables (Jahreis, 2015; Tibshirani, 1996; Zou and Hastie, 2005). The penalty parameter is called λ. If λ is zero, the lasso estimator will be the same as an ordinary least squares estimator that includes all the variables and only minimizes the residuals. On the contrary, large values of λ will assign zero to all the coefficients (Jahreis, 2015). Using a cross validation method can simplify the process of choosing a moderate λ value which is necessary for proper variable selection (Hastie, 2009).

## 3. RESULTS

To show the variations among the realizations, as shown in Figure 1 (a)-(b), four random realizations were chosen out of ten simulation sets for standard deviations of 1123 and 11232 with major and minor anisotropy directions of 100 mm and 50 mm, respectively. The simulations were all carried out with a flow rate of 5 ml/min and a transverse dispersivity of 0.005 (cm). The realization sets with standard deviation of 1123, Figure 1 (c), demonstrates that in spite of the significant differences in the spatial distribution of the realizations, the breakthrough curves are very similar to one another. However, it can be observed in Figure 1 (d) that the breakthrough curves are significantly dissimilar. This disparity is due to high standard deviation values which result in a larger permeability variation in each simulation set; thus, the effect of spatial distribution becomes more pronounced. However, spatial distribution does not seem to have a significant impact on the breakthrough curves in lower standard deviations simply because the variation between the values is so small that the spatial distribution of those values has no effect.

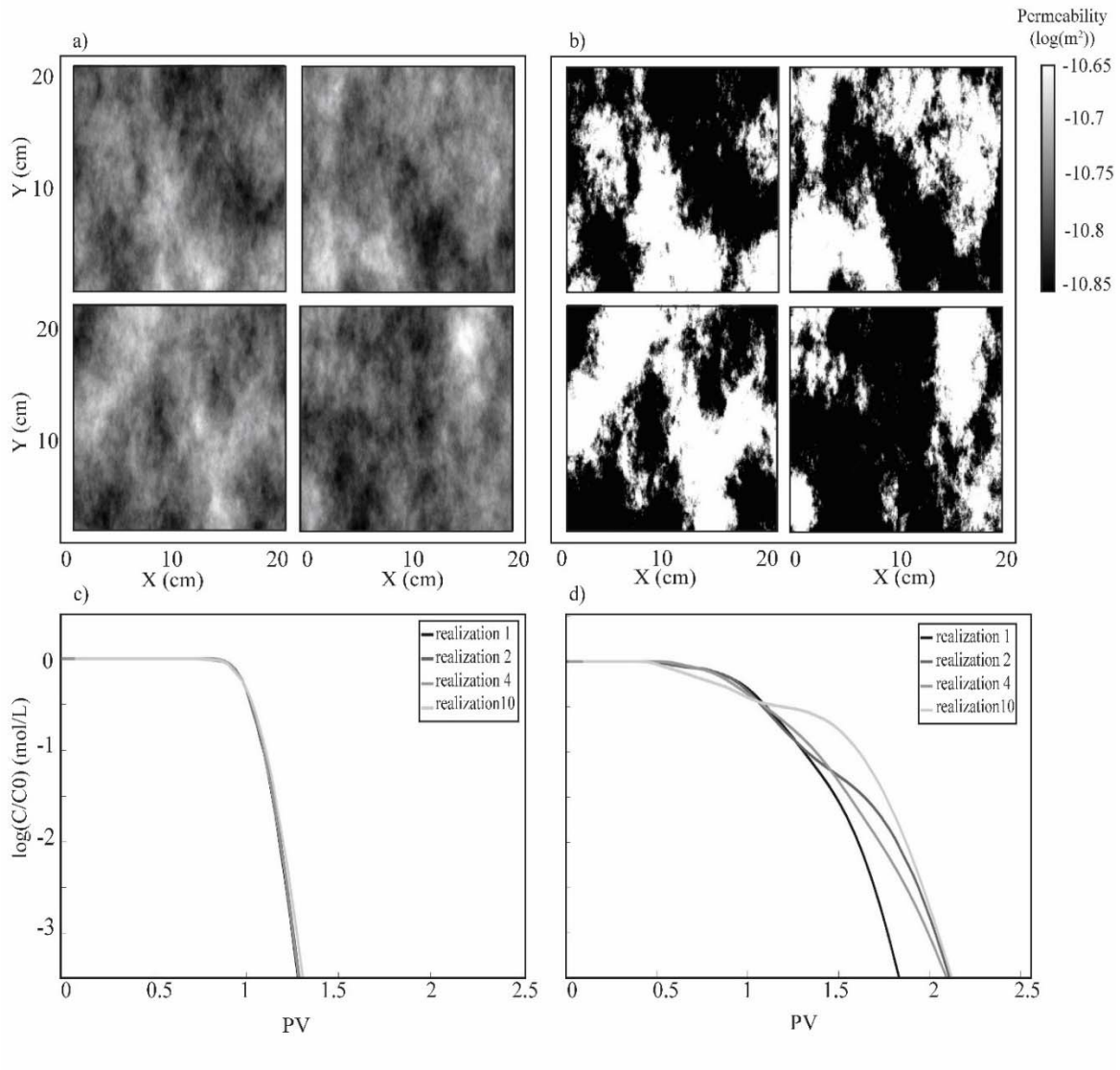


Figure 1. 2D Spatial profiles of different realizations: (a) the permeability spatial distribution with standard deviation of 1123, (b) the permeability spatial distribution with standard deviation of 11232, (c) average breakthrough curves for four realizations with standard deviation of 1123 and (d) breakthrough curves for four realizations with standard deviation of 11232.

## 3.1. EFFECT OF PERMEABILITY STANDARD DEVIATION

The effect of standard deviation variations on solute transport and the attenuation time were examined. Figure 2 (a)-(c) demonstrates the permeability spatial distribution in

three simulations set that were selected randomly. Standard deviation in columns (I) through (II) is 112, 1123 and 11232. Figure 2 (d)-(f) shows Br concentration profiles at 0.5 pore volumes. Figure 2 (g)-(i) shows the velocity profile at 0.5 pore volumes. As expected, it can be seen that the lowest standard deviation has the lowest velocity and lowest velocity variation throughout the porous media. Figure 2 (j) shows the overall breakthrough curves for different standard deviation values. We analyzed ten realizations for each simulation sets and plotted the average of those ten realizations and the standard deviation of the values are represented by error bars. Increase in permeability standard deviation results in increase in attenuation time. However this change is more pronounce when the standard deviation was increased from 1123 to 11232.

As shown in Figure 2 (a)-(c), lower standard deviation resembles a well-mixed or homogenous medium and the permeability variability is really low. Whereas for larger values for standard deviation the variability becomes much larger and the medium becomes highly heterogeneous with very high variation in permeability values. Velocity profile Figure 2 (g)-(i) also demonstrates in column (I) which has a low standard deviation , velocity is almost the same throughout the profile therefore the Br concentration front is very smooth, however as the standard deviation increase it can be observed that the front becomes very uneven and it follows the permeability and velocity profile pattern. In the zones with higher permeability and velocity the concentration has significantly decreased.

Interestingly, it can be observed in Figure 2 (j) that initially the concentration starts to decrease faster in high standard deviation condition but the breakthrough happens much faster in the media with lower standard deviation. The high contrast in

permeability values of each point in the media when the standard deviation is high cause tailing in the breakthrough curves. Meaning that, it takes longer (more pore volumes) for the fluid to pass through whereas in lower standard deviation the contrast between permeability values of the medium is lower therefore the fluid flushes out with a steady rate throughout the media.

## 3.2. EFFECT OF FLOW

In order to examine the effect of flow rate and permeability standard deviation on attenuation time, as shown in Figure 3 the breakthrough curves are plotted for each flow rate under low, medium and high standard deviation (112, 1123, 11232) . As the flow rate increase the advection part of ADE Eq (1) becomes larger which will result in a faster concentration reduction. However, it will simultaneously increase the mechanical dispersion and the ultimately increase the dispersion coefficient (Eq (2) and (3)). Thus, higher flow which will result in a more pronounced dispersion values which result in tailing of the breakthrough. Therefore, the changes are negligible when the flow rate increases from 5 to 25 (ml/min). As it is shown in Figure 3 (a)-(c), by increasing the permeability standard deviation changes between the breakthrough curves with different flow rate will not become any more significant and the trend remains the same for medium and high standard deviation. The slope of the breakthrough curves with the highest standard deviation decrease significantly due to the fact that the permeability field becomes more heterogeneous and the variability between each point becomes larger therefore it takes longer for the fluid to progress in the media.

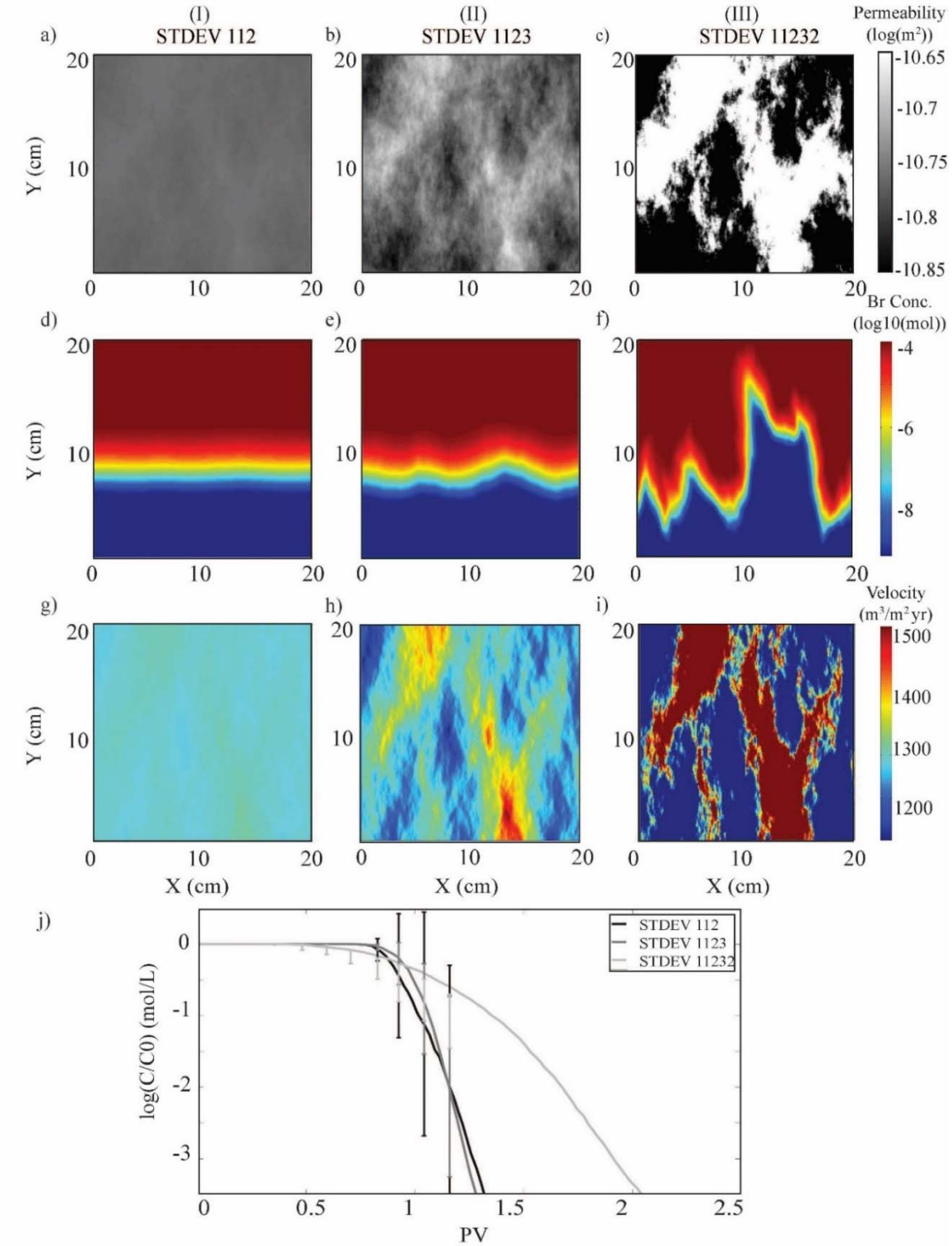


Figure 2. 2D Spatial profiles of Br transport under various standard deviations (112, 1123, 11232) : (a) – (c) the permeability spatial distribution, (d)-(f) Br concentration front at 0.5 pore volumes, (g)-(i) velocity profile, (j) concentration of Br.

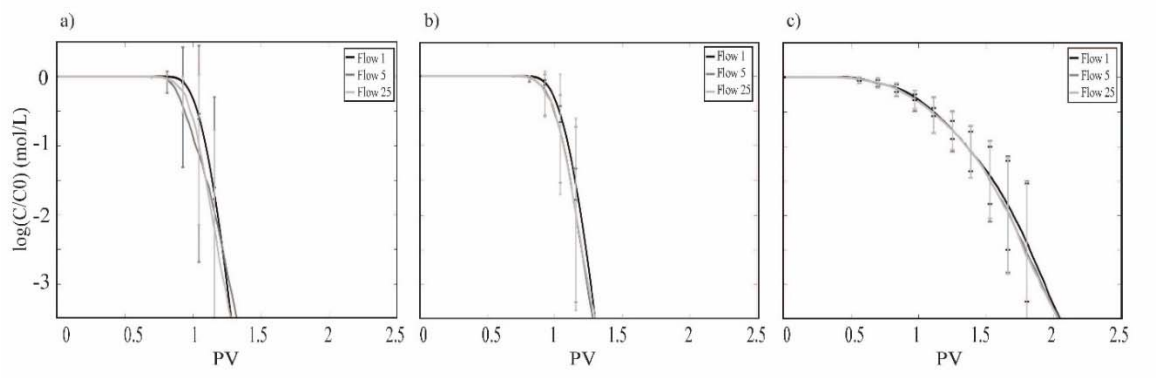


Figure 3. Br breakthrough curves under different flow rates with low to high standard deviation: a) low standard deviation (112), b) medium standard deviation (1123) and c) high standard deviation (11232).

## 3.3. EFFECT OF MAJOR ANISOTROPY

The effect of different major anisotropies (variogram range) on attenuation time was studied in this section. Figure 4 (a)-(c) describe the 2D spatial distribution of permeability with standard deviation of 11232, respectively. Figure 4 (d)-(f) demonstrate Br concentration profiles. To illustrate the effect of major anisotropy , minor anisotropy was kept at 20 mm and major anisotropy values was set to 20 , 50 and 100 mm column (I) to (II), respectively. Figure 4 (g)-(i) show the velocity profile. As the major anisotropy increases the porous media move further away from homogenous distribution. Therefore, with the increase in major anisotropy values the Br concentration front becomes more uneven. However this uneven and rough concentration front is less significant in low standard deviation and becomes more pronounce when the permeability standard deviation is the highest (Figure 4 (d)-(f)).

Similarly, the effect of inclination in major anisotropy values on breakthrough curves are more noticeable when standard deviation is high, as shown in Figure 5 (a)-(c).

Lower anisotropy values resemble a more homogenous or well mixed porous media therefore the concentration decreases much faster than the high major anisotropy value. This tailing is due to the fact that higher major anisotropy increase the distance that permeability values are correlated which will lead to zonation happening in major anisotropy direction and therefore causing a delay in breakthrough. The same trend applies to the breakthrough curves with lower permeability standard deviation values even though it is not as distinguishable as higher permeability standard deviation. However, bear in mind that when the variability between the values are small, the spatial distribution and the distance in which the values are correlated does not come into effect. In other words, the effect of major anisotropy direction will be significant only if the variation between the values are high.

### 3.4. EFFECT OF MINOR ANISOTROPY

In addition to major direction anisotropy, the effect of minor anisotropy which is perpendicular to the flow was also examined. Figure 6 (a)-(c) illustrate the 2D spatial distribution of permeability with standard deviation of 11232. In order to investigate the effect of minor direction anisotropy, major anisotropy was kept constant at 100 mm and minor anisotropy was increased from 10 mm to 50mm (column (I)-(II)). As shown in Figure 6 (g)-(i) the high velocity zones and high permeability zones are highly compatible and the zones becomes wider as the minor anisotropy values increases. It can be observed in Figure 6 (d)-(f) that the Br concentration front becomes smoother as the value for values for minor anisotropy increases and it comes closer to major direction anisotropy value.

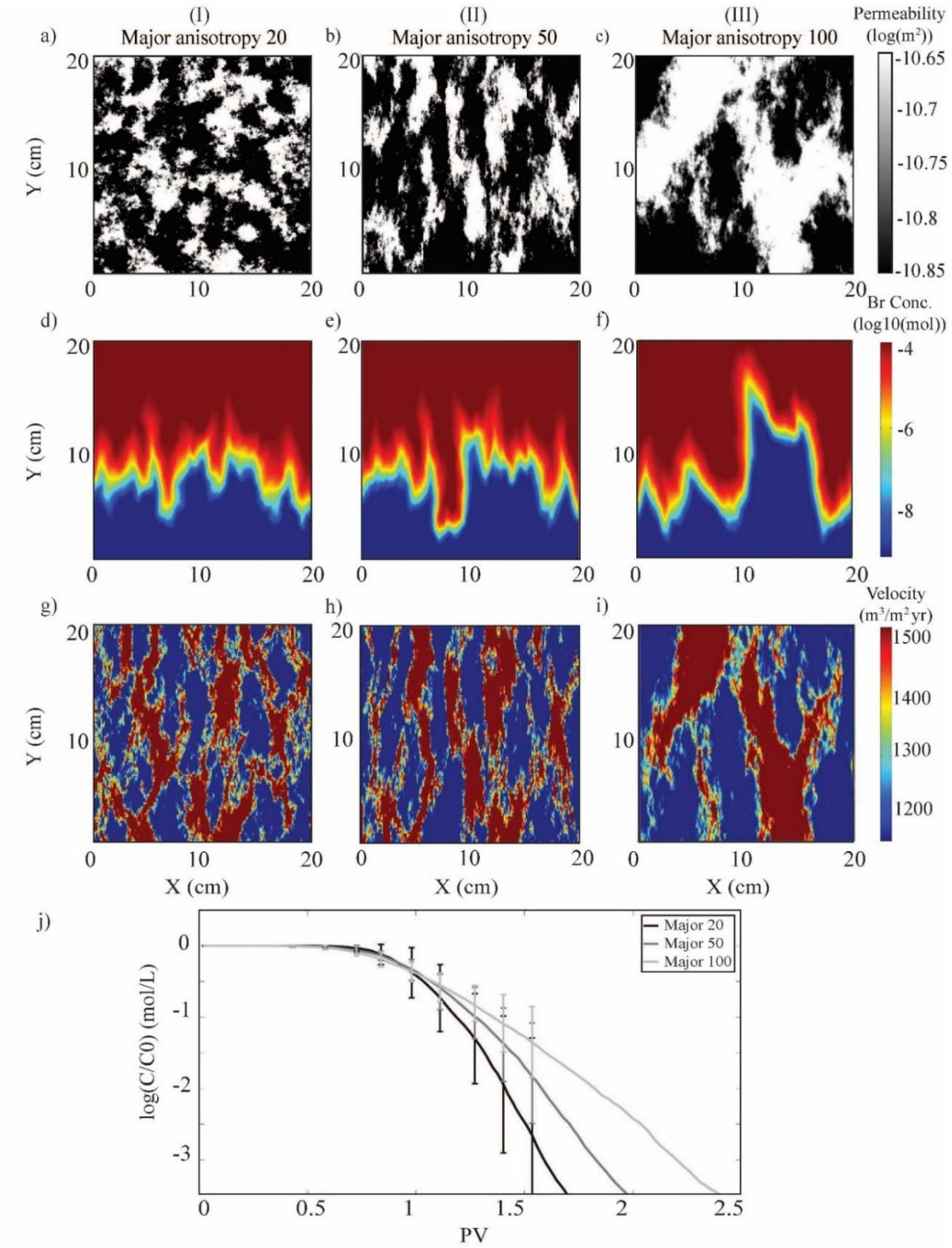


Figure 4. 2D Spatial profiles of Br transport under various major direction anisotropy values (20, 50, 100) : (a) – (c) the permeability spatial distribution, (d)-(f) Br concentration front at 0.5 pore volumes, (g)-(i) velocity profile, (j) concentration of Br.

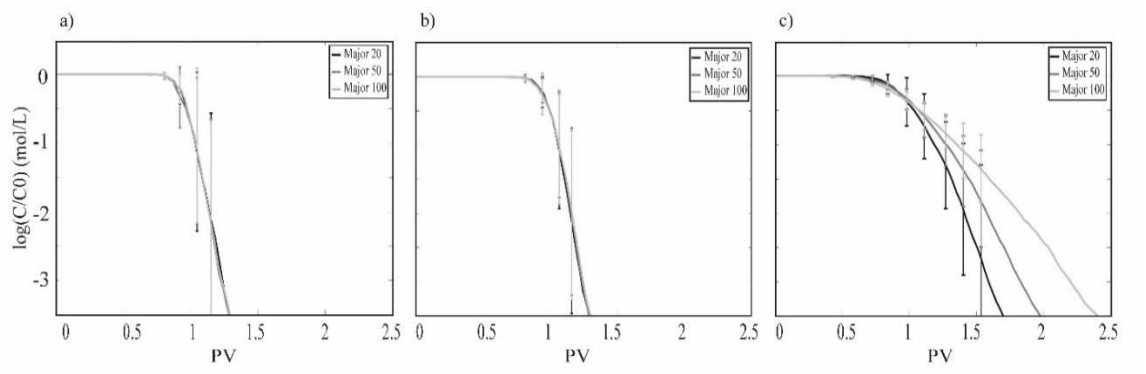


Figure 5. Br breakthrough curves for different major direction anisotropies with low to high standard deviation: a) low standard deviation (112), b) medium standard deviation (1123) and c) high standard deviation (11232).

When the two anisotropy direction are equal, the medium resembles an isotropic well mixed media.

Similar to major anisotropy values, the effect of minor anisotropy is not very pronounce when the standard deviation is the low (1123). However, for greater standard deviation values the difference between the minor anisotropy values becomes significant. As it is shown in Figure 6 (j) the largest minor anisotropy has the fastest concentration reduction. Whereas Br concentration in simulations with smaller values of minor anisotropy take much longer to decrease.

It can be derived from Figure 7 (a)-(c) that the time delay in breakthrough curves is highly dependent on the difference between the major and minor anisotropy values. In lower minor anisotropy values, narrow high permeability zones (channels) occur along the direction of the flow. Within the high permeability and high velocity channels concentration decrease rapidly. However due preferential flow paths, the fluid does not progress outside of the channels as much as it does within them. Since there is much lower flow out side of the channels the concentration in low permeability zones will not decrease.

The breakthrough tailing and delay in concentration reduction decrease as minor anisotropy increases because the high permeability zones becomes wider and channeling is significantly reduced.

## 3.5. EFFECT OF TRANSVERSE DISPERSIVITY

In order to examine the effect of transverse dispersivity and permeability standard deviation on attenuation time, the breakthrough curves are plotted for each transverse dispersivity under low, medium and high standard deviation as shown in Figure 8 The transverse dispersivity values increases from 0.001 to 0.005 and then eventually to 0.01 (cm). It can be observed in Figure 8 (a)-(c) that as the standard deviation increases the disparity between the breakthrough curves lessens. As shown in Figure 8 (a), in permeability field with low standard deviation the effect of transverse dispersivity is more significant. The changes are trivial when the transverse dispersivity is increased from 0.001 to 0.005 (cm). However, when it increases to 0.05, the slope of the breakthrough curve decreases. In other words, as the transverse dispersivity increases, the concentration reduction becomes slower and the attenuation time increases.

Higher transverse dispersivity values will increase the mechanical dispersion perpendicular to the flow direction Eq (3). This causes the flow to disperse more in perpendicular direction, therefore it takes longer for the fluid to progress in media in the direction of flow and flush out of the porous medium. Thus, the concentration reduction occurs with a slightly lower pace. It is noteworthy to mention that the same trend applies to the breakthrough curves for higher standard deviations. However, it appears that in higher standard deviation the effect of the changes in transverse dispersivity is negligible.

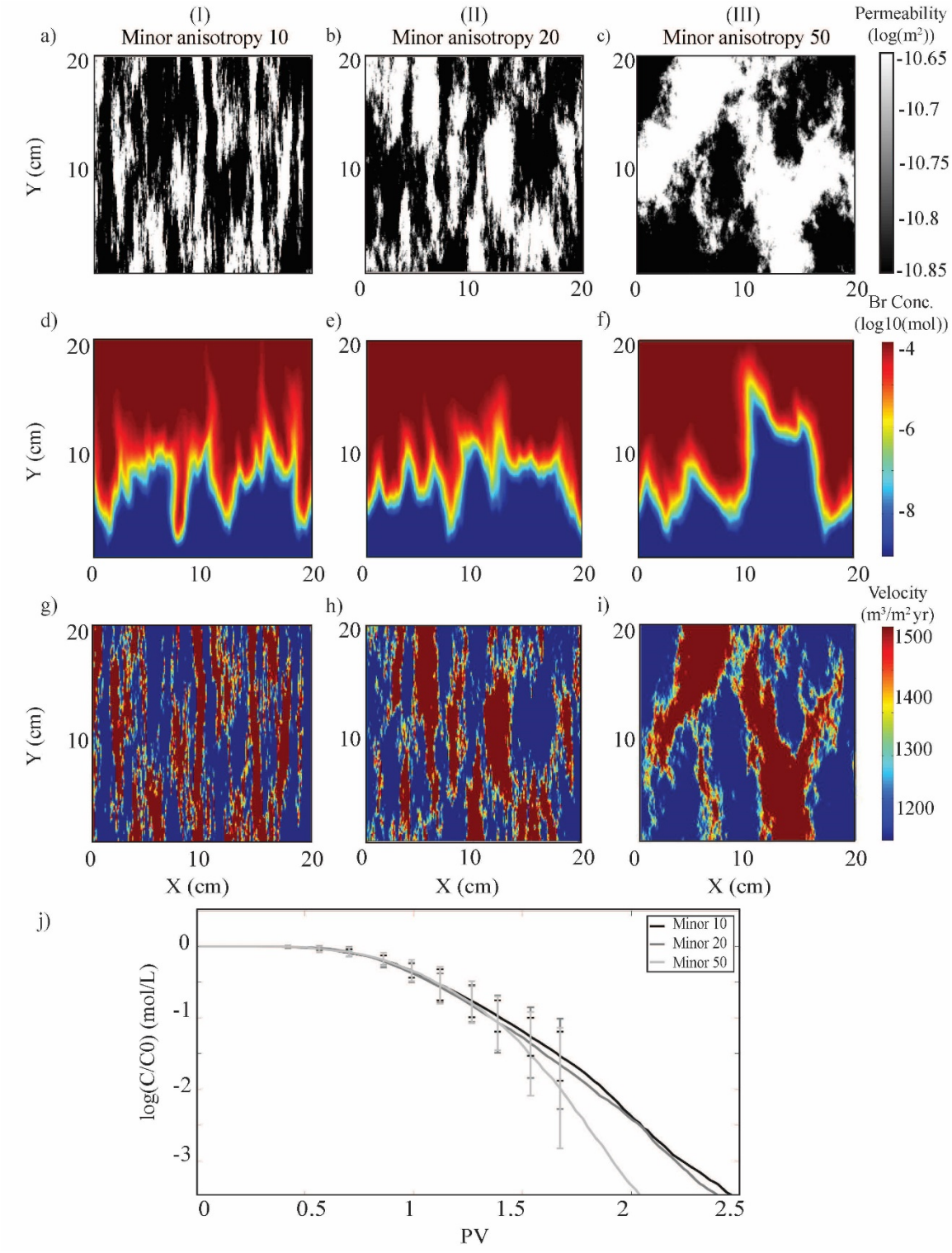


Figure 6. 2D Spatial profiles of Br transport under various minor direction anisotropy values (10, 20, 50) : (a) – (c) the permeability spatial distribution, (d)-(f) Br concentration front at 0.5 pore volumes, (g)-(i) velocity profile, (j) concentration of Br.

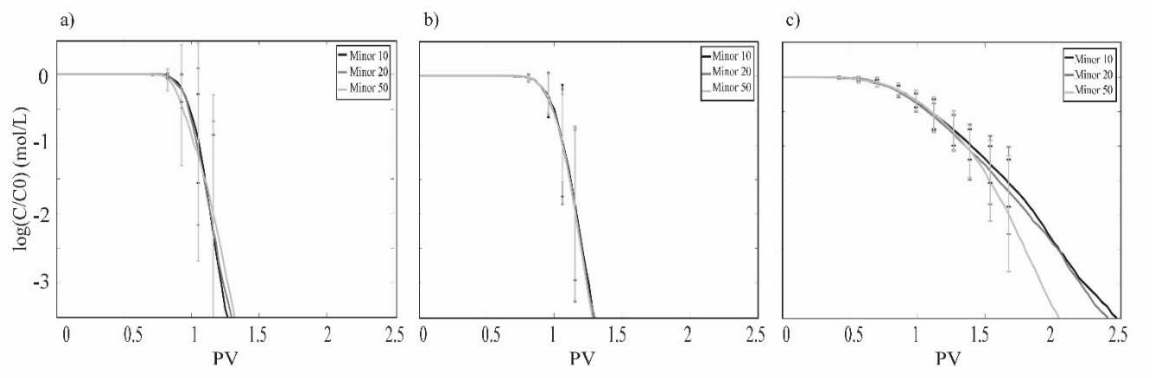


Figure 7. Br breakthrough curves for different minor direction anisotropies with low to high standard deviation: a) low standard deviation (112), b) medium standard deviation (1123) and c) high standard deviation (11232).

In comparison with high standard deviation, the velocity distribution under lower standard deviation conditions is relatively more uniform and has much lower magnitude. Thus, since the advection part of the ADE is relatively smaller the dispersion section is more dominant, the changes in transverse dispersivity tend to be more significant in lower standard deviations. Whereas, in higher standard deviations the velocity and its variation is high, therefore the advection part of the ADE is more dominant and the changes in the dispersion part is negligible.

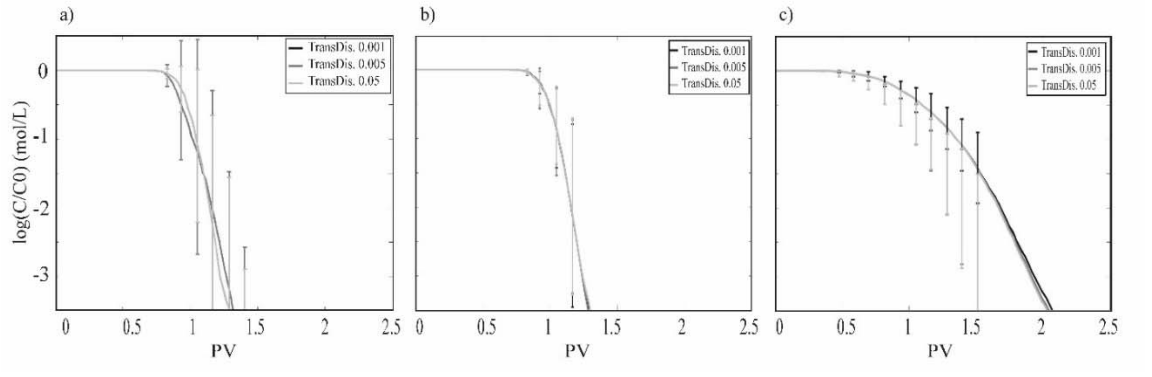


Figure 8. Br breakthrough curves for different transverse dispersivities with low to high standard deviation: a) low standard deviation (112), b) medium standard deviation (1123) and c) high standard deviation (11232).

## 3.6. FEATURE SELECTION AND REGRESSION

The pore volume at which concentration reaches 0.01 of the initial condition was chosen as the dependent variable. The standard deviation, flow rate, transverse dispersivity, and major and minor direction anisotropy were the independent variables. In order to capture non-linearity in the initial variables, the functions, $x^2, x^3, x^4, \frac{1}{x}, 10^x, 10^{-x}, log\ (x), ln(x), \sqrt[2]{x}, \sqrt[3]{x}$ were used to transform the data. After transformation, the variables in were divided in training, validation, and test datasets and then were standardized using the training dataset. The feature selection was conducted with the lassoCV (cross validation code) function from Python's Scikit-learn package. The code used the data to determine the L1 penalty coefficient and λ. The most significant variables and their coefficients are presented in Table 3, with λ = 0.001275.

After feature selection, simple linear regression was performed and in order to provide a more realistic estimate of accuracy each model need to be verified using the test dataset (never used during training), which resulted in an $R^2$ score 0.7083, meaning that 70.83% of the data can be explained by the model.

Table 3. Coefficients calculated from regression analysis

| **Variable** | **Lasso coefficients** | **Regression coefficients** |
|---|---|---|
| **Transverse dispersivity** | -0.00084 | -3.7E+10 |
| **Transverse dispersivity $^2$** | -7.17E-14 | -6.6E+11 |
| **Transverse dispersivity $^3$** | -6.70E-15 | 2.96E+11 |
| **10 $^{-Dispersivity}$** | 1.20E-12 | -4E+11 |
| **Mean Permeability $^4$** | 1.273547 | 2.13E+08 |
| **log10 (Mean Permeability)** | 3.80E-15 | 34133382 |
| **Ln (Mean Permeability)** | -1.97E-17 | 1.9E+08 |
| **Mean Permeability $^{0.5}$** | -1.97E-17 | 2.21E+08 |
| **Mean Permeability $^{0.33}$** | -1.97E-17 | -6.4E+07 |

Table 3. Coefficients calculated from regression analysis (Cont.)

| | | |
|---|---|---|
| **STDV Permeability** | 0.057603 | 14272288 |
| **STDV Permeability $^{2}$** | 0.098959 | -1.5E+09 |
| **STDV Permeability $^{3}$** | 0.010085 | 1.48E+10 |
| **STDV Permeability $^{4}$** | 0.00101 | -1.3E+10 |
| **Major Anisotropy** | 0.034596 | 0.0401 |
| **10 $^{\text{Major Anisotropy}}$** | -0.00428 | -0.00418 |
| **Major Anisotropy $^{0.5}$** | 0.006665 | 0.003418 |
| **Minor Anisotropy** | -0.00993 | -0.04849 |
| **Minor Anisotropy $^{2}$** | -0.00237 | 0.02491 |
| **10 $^{\text{Minor Anisotropy}}$** | -0.00297 | -0.01331 |
| **Minor Anisotropy $^{-1}$** | -0.02365 | -0.02969 |

## 4. DISCUSSION AND CONCLUSIONS

This work investigates the effect of physical heterogeneity on Br attenuation time. Porous media were generated using statistical parameters such as permeability mean, permeability standard deviation, major direction anisotropy and minor direction anisotropy. The simulations were performed under different flow rates and transverse dispersivity values. A total of 3536 simulations were carried out.

The longest it took for the concentration to decrease to 0.1 of the initial concentration is 1.90578 pore volumes, which was obtained under the following condition, flow rate of 5 (ml/min), standard deviation of 11232, major direction anisotropy of 100 mm and minor direction anisotropy of 50 mm. The fastest concentration reduction to 0.1 of the initial concentration is at 1.08673 pore volumes, which occurred under the lowest standard deviation (11), flow rate of 25 (ml/min) and major direction anisotropy and minor direction anisotropy of 1 mm.

Overall standard deviation had the most significant impact on the attenuation time, followed by major and minor anisotropy. With 99 % decrease in permeability standard deviation values, the attenuation time for concentration to decrease to 0.1 of the initial concentration, decreases by 20%. It can also be observed that the effect of major and minor anisotropy is only significant when the standard deviation is the highest. Under that condition, with 80% decrease in major direction anisotropy values the attenuation time decreases by 11%. Similarly, by 80% decrease in minor direction anisotropy values the attenuation time increases by 1.37%. Interestingly, changes in transverse dispersivity only comes into effect when the standard deviation is very low, Even though changing the flow rate and dispersivity have some effects on the attenuation time, it seems to be significantly less effective in comparison with other parameters.

Lasso regression was used to select the most significant variables and simple linear regression was conducted on the selected variables in attempt to find the best fitting model. The model then was verified on the test data set which resulted in $R^2$ score of 0.7083. It can be concluded that due to the fact that controlling the media's characteristic is very complex in the laboratory, numerical studies proven to be successful in modeling the solute transport in a vast variety of porous media.

## REFERENCES

Adams, E. E., and L. W. Gelhar (1992), FIELD-STUDY OF DISPERSION IN A HETEROGENEOUS AQUIFER .2. SPATIAL MOMENTS ANALYSIS, *Water Resources Research*, *28*(12), 3293-3307.

Allen-King, R. M., R. M. Halket, D. R. Gaylord, and M. J. L. Robin (1998), Characterizing the heterogeneity and correlation of perchloroethene sorption and hydraulic conductivity using a facies-based approach, *Water Resources Research*, *34*(3), 385-396.

Babadagli, T. (2006), Effective permeability estimation for 2-D fractal permeability fields, *Mathematical Geology*, *38*(1), 33-50.

Bao, C., H. Wu, L. Li, D. Newcomer, P. E. Long, and K. H. Williams (2014), Uranium Bioreduction Rates across Scales: Biogeochemical Hot Moments and Hot Spots during a Biostimulation Experiment at Rifle, Colorado, *Environ. Sci. Technol.*, *48*(17), 10116-10127.

Barber, L. B., E. M. Thurman, and D. D. Runnells (1992), Geochemical heterogeneity in a sand and gravel aquifer: Effect of sediment mineralogy and particle size on the sorption of chlorobenzenes, *Journal of Contaminant Hydrology*, *9*(1), 35-54.

Bear, J. (1988), Dynamics of fluids in porous media, edited, Dover, New York.

Benson, D. A., S. W. Wheatcraft, and M. M. Meerschaert (2000a), Application of a fractional advection-dispersion equation, *Water Resources Research*, *36*(6), 1403-1412.

Benson, D. A., S. W. Wheatcraft, and M. M. Meerschaert (2000b), The fractional-order governing equation of Levy motion, *Water Resources Research*, *36*(6), 1413-1423.

Berkowitz, B., and H. Scher (1998), Theory of anomalous chemical transport in random fracture networks, *Physical Review E*, *57*(5), 5858-5869.

Berkowitz, B., and H. Scher (2001), The role of probabilistic approaches to transport theory in heterogeneous media, *Transport in Porous Media*, *42*(1-2), 241-263.

Berkowitz, B., H. Scher, and S. E. Silliman (2000), Anomalous transport in laboratory-scale, heterogeneous porous media, *Water Resources Research*, *36*(1), 149-158.

Berkowitz, B., A. Cortis, M. Dentz, and H. Scher (2006), Modeling non-Fickian transport in geological formations as a continuous time random walk, *Reviews of Geophysics*, *44*(2).

Bernabe, Y., U. Mok, and B. Evans (2003), Permeability-porosity relationships in rocks subjected to various evolution processes, *Pure and Applied Geophysics*, *160*(5-6), 937-960.

Bernabe, Y., U. Mok, B. Evans, and F. J. Herrmann (2004), Permeability and storativity of binary mixtures of high- and low-permeability materials, *Journal of Geophysical Research-Solid Earth*, *109*(B12).

Bernabe, Y., M. Zamora, M. Li, A. Maineult, and Y. B. Tang (2011), Pore connectivity, permeability, and electrical formation factor: A new model and comparison to experimental data, *Journal of Geophysical Research-Solid Earth*, *116*.

Bohling, G. (2005), Introduction to geostatistics and variogram analysis, *Kansas geological survey, 20p*.

Brusseau, M. L., R. E. Jessup, and P. S. C. Rao (1989), Modeling the transport of solutes influenced by multiprocess nonequilibrium, *Water Resources Research*, *25*(9), 1971-1988.

Chao, H. C., H. Rajaram, and T. Illangasekare (2000), Intermediate-scale experiments and numerical simulations of transport under radial flow in a two-dimensional heterogeneous porous medium, *Water Resources Research*, *36*(10), 2869-2884.

Cortis, A., and B. Berkowitz (2004), Anomalous transport in "classical" soil and sand columns, *Soil Science Society of America Journal*, *68*(5), 1539-1548.

Dagan, G. (1990), TRANSPORT IN HETEROGENEOUS POROUS FORMATIONS - SPATIAL MOMENTS, ERGODICITY, AND EFFECTIVE DISPERSION, *Water Resources Research*, *26*(6), 1281-1290.

Dagan, G. (2004), On application of stochastic modeling of groundwater flow and transport, *Stochastic Environmental Research and Risk Assessment*, *18*(4), 266-267.

Dagan, G., A. Fiori, and I. Jankovic (2013), Upscaling of flow in heterogeneous porous formations: Critical examination and issues of principle, *Adv. Water Resour.*, *51*, 67-85.

de Dreuzy, J.-R., and P. Davy (2007), Relation between fractional flow models and fractal or long-range 2-D permeability fields, *Water Resources Research*, *43*(4), n/a-n/a.

de Marsily, G., F. Delay, J. Goncalves, P. Renard, V. Teles, and S. Violette (2005), Dealing with spatial heterogeneity, *Hydrogeology Journal*, *13*(1), 161-183.

Dentz, M., A. Cortis, H. Scher, and B. Berkowitz (2004), Time behavior of solute transport in heterogeneous media: transition from anomalous to normal transport, *Adv. Water Resour.*, *27*(2), 155-173.

Desbarats, A. J., and S. Bachu (1994), GEOSTATISTICAL ANALYSIS OF AQUIFER HETEROGENEITY FROM THE CORE SCALE TO THE BASIN-SCALE - A CASE-STUDY, *Water Resources Research*, *30*(3), 673-684.

Di Federico, V., M. Pinelli, and R. Ugarelli (2010), Estimates of effective permeability for non-Newtonian fluid flow in randomly heterogeneous porous media, *Stochastic Environmental Research and Risk Assessment*, *24*(7), 1067-1076.

Fernandez-Garcia, D., T. H. Illangasekare, and H. Rajaram (2005), Differences in the scale-dependence of dispersivity estimated from temporal and spatial moments in chemically and physically heterogeneous porous media, *Adv. Water Resour.*, *28*(7), 745-759.

Frank, I. E., and J. H. Friedman (1993), A STATISTICAL VIEW OF SOME CHEMOMETRICS REGRESSION TOOLS, *Technometrics*, *35*(2), 109-135.

Garabedian, S. P., D. R. Leblanc, L. W. Gelhar, and M. A. Celia (1991), LARGE-SCALE NATURAL GRADIENT TRACER TEST IN SAND AND GRAVEL, CAPE-COD, MASSACHUSETTS .2. ANALYSIS OF SPATIAL MOMENTS FOR A NONREACTIVE TRACER, *Water Resources Research*, *27*(5), 911-924.

Gelhar, L. W. (1986), Stochastic subsurface hydrology from theory to applications, *Water Resources Research*, *22*(9S), 135S-145S.

Gelhar, L. W., C. Welty, and K. R. Rehfeldt (1992), A CRITICAL-REVIEW OF DATA ON FIELD-SCALE DISPERSION IN AQUIFERS, *Water Resources Research*, *28*(7), 1955-1974.

Gerke, H. H., and M. T. Vangenuchten (1993), A DUAL-POROSITY MODEL FOR SIMULATING THE PREFERENTIAL MOVEMENT OF WATER AND SOLUTES IN STRUCTURED POROUS-MEDIA, *Water Resources Research*, *29*(2), 305-319.

Gjetvaj, F., A. Russian, P. Gouze, and M. Dentz (2015), Dual control of flow field heterogeneity and immobile porosity on non-Fickian transport in Berea sandstone, *Water Resources Research*, *51*(10), 8273-8293.

Goltz, M. N., and P. V. Roberts (1986), Three-Dimensional Solutions for Solute Transport in an Infinite Medium With Mobile and Immobile Zones, *Water Resources Research*, *22*(7), 1139-1148.

Gouze, P., Y. Melean, T. Le Borgne, M. Dentz, and J. Carrera (2008), Non-Fickian dispersion in porous media explained by heterogeneous microscale matrix diffusion, *Water Resources Research*, *44*(11), n/a-n/a.

Gringarten, E., and C. V. Deutsch (2001), Teacher's Aide Variogram Interpretation and Modeling, *Mathematical Geology*, *33*(4), 507-534.

Haggerty, R., and S. M. Gorelick (1995), MULTIPLE-RATE MASS-TRANSFER FOR MODELING DIFFUSION AND SURFACE-REACTIONS IN MEDIA WITH PORE-SCALE HETEROGENEITY, *Water Resources Research*, *31*(10), 2383-2400.

Hastie, T., Tibshirani, R. and Friedman, J. (2009), Elements of Statistical Learning: Data Mining, Inference and Prediction, *New York: Springer*, *2nd edn*.

Heidari, P., and L. Li (2014a), Solute transport in low-heterogeneity sandboxes: The role of correlation length and permeability variance, *Water Resources Research*, *50*(10), 8240-8264.

Heidari, P., and L. Li (2014b), Solute transport in low-heterogeneity sand boxes: The role of correlation length and permeability variance, *Water Resources Research*, *50*(10), 8240-8264.

Hoerl, A. E., and R. W. Kennard (2004), Ridge Regression, in *Encyclopedia of Statistical Sciences*, edited, John Wiley & Sons, Inc.

Jahreis, K. (2015), Measurement Error in LASSO-Analytical Results and a Simulation Study.

Jankovic, I., A. Fiori, and G. Dagan (2003), Flow and transport in highly heterogeneous formations: 3. Numerical simulations and comparison with theoretical results, *Water Resources Research*, *39*(9).

Jankowski, J., and P. Beck (2000), Aquifer heterogeneity: hydrogeological and hydrochemical properties of the Botany Sands aquifer and their impact on contaminant transport, *Australian Journal of Earth Sciences*, *47*(1), 45-64.

Jin, L., R. Mathur, G. Rother, D. Cole, E. Bazilevskaya, J. Williams, A. Carone, and S. Brantley (2013), Evolution of porosity and geochemistry in Marcellus Formation black shale during weathering, *Chemical Geology*, *356*, 50-63.

Landrot, G., J. B. Ajo-Franklin, L. Yang, S. Cabrini, and C. I. Steefel (2012), Measurement of accessible reactive surface area in a sandstone, with application to CO2 mineralization, *Chemical Geology*, *318*, 113-125.

Levy, M., and B. Berkowitz (2003), Measurement and analysis of non-Fickian dispersion in heterogeneous porous media, *Journal of Contaminant Hydrology*, *64*(3-4), 203-226.

Li, L., N. Gawande, M. B. Kowalsky, C. I. Steefel, and S. S. Hubbard (2011), Physicochemical Heterogeneity Controls on Uranium Bioreduction Rates at the Field Scale, *Environ. Sci. Technol.*, *45*(23), 9959-9966.

Maher, K., C. I. Steefel, A. F. White, and D. A. Stonestrom (2009), The role of reaction affinity and secondary minerals in regulating chemical weathering rates at the Santa Cruz Soil Chronosequence, California, *Geochim. Cosmochim. Acta*, *73*(10), 2804-2831.

Manto, H. (2005), Modelling of geometric anisotropic spatial variation, *Mathematical Modelling and Analysis*, 361-366.

Meerschaert Mark, M., and A. Sikorskii (2011), *Stochastic Models for Fractional Calculus*.

Meerschaert, M. M., D. A. Benson, and B. Baumer (1999), Multidimensional advection and fractional dispersion, *Physical Review E*, *59*(5), 5026-5028.

Meinshausen, N., and P. Bühlmann (2006), High-dimensional graphs and variable selection with the lasso, *The annals of statistics*, 1436-1462.

Nicolaides, C., B. Jha, L. Cueto-Felgueroso, and R. Juanes (2015), Impact of viscous fingering and permeability heterogeneity on fluid mixing in porous media, *Water Resources Research*, *51*(4), 2634-2647.

Pedretti, D., D. Fernandez-Garcia, D. Bolster, and X. Sanchez-Vila (2013), On the formation of breakthrough curves tailing during convergent flow tracer tests in three-dimensional heterogeneous aquifers, *Water Resources Research*, *49*(7), 4157-4173.

Pedretti, D., A. Molinari, C. Fallico, and S. Guzzi (2016), Implications of the change in confinement status of a heterogeneous aquifer for scale-dependent dispersion and mass-transfer processes, *Journal of Contaminant Hydrology*, *193*, 86-95.

Ramasomanana, F., A. Younes, and P. Ackerer (2013), Estimation of macrodispersion in 2-D highly heterogeneous porous media using the Eulerian-Lagrangian localized adjoint method, *Water Resources Research*, *49*(1), 43-53.

Renard, P., and G. deMarsily (1997), Calculating equivalent permeability: A review, *Adv. Water Resour.*, *20*(5-6), 253-278.

Renard, P., and D. Allard (2013), Connectivity metrics for subsurface flow and transport, *Adv. Water Resour.*, *51*, 168-196.

Russo, D., and M. Bouton (1992), Statistical analysis of spatial variability in unsaturated flow parameters, *Water Resources Research*, *28*(7), 1911-1925.

Scheibe, T. D., S. S. Hubbard, T. C. Onstott, and M. F. DeFlaun (2011), Lessons Learned from Bacterial Transport Research at the South Oyster Site, *Ground Water*, *49*(5), 745-763.

SHARMA, P. K., and T. A. ABGAZE (2015), Solute transport through porous media using asymptotic dispersivity, *Sadhana*, *40*(5), 1595-1609.

Silliman, S. E. (2001), Laboratory study of chemical transport to wells within heterogeneous porous media, *Water Resources Research*, *37*(7), 1883-1892.

Singha, K., L. Li, F. D. Day-Lewis, and A. B. Regberg (2011), Quantifying solute transport processes: Are chemically "conservative" tracers electrically conservative?, *Geophysics*, *76*(1), F53-F63.

Song, I., and J. Renner (2006), Experimental investigation into the scale dependence of fluid transport in heterogeneous rocks, *Pure and Applied Geophysics*, *163*(10), 2103-2123.

Steefel, C. I., and P. C. Lichtner (1994), Diffusion and reaction in rock matrix bordering a hyperalkaline fluid-filled fracture, *Geochim. Cosmochim. Acta*, *58*(17), 3595-3612.

Steefel, C. I., S. Carroll, P. H. Zhao, and S. Roberts (2003), Cesium migration in Hanford sediment: a multisite cation exchange model based on laboratory transport experiments, *Journal of Contaminant Hydrology*, *67*(1-4), 219-246.

Sudicky, E. A., W. A. Illman, I. K. Goltz, J. J. Adams, and R. G. McLaren (2010a), Heterogeneity in hydraulic conductivity and its role on the macroscale transport of a solute plume: From measurements to a practical application of stochastic flow and transport theory, *Water Resources Research*, *46*(1), n/a-n/a.

Sudicky, E. A., W. A. Illman, I. K. Goltz, J. J. Adams, and R. G. McLaren (2010b), Heterogeneity in hydraulic conductivity and its role on the macroscale transport of a solute plume: From measurements to a practical application of stochastic flow and transport theory, *Water Resources Research*, *46*.

Sun, W. C., J. E. Andrade, and J. W. Rudnicki (2011), Multiscale method for characterization of porous microstructures and their impact on macroscopic effective permeability, *International Journal for Numerical Methods in Engineering*, *88*(12), 1260-1279.

Tibshirani, R. (1996), Regression shrinkage and selection via the Lasso, *J. R. Stat. Soc. Ser. B-Methodol.*, *58*(1), 267-288.

Valocchi, A. J. (1985), Validity of the Local Equilibrium Assumption for Modeling Sorbing Solute Transport Through Homogeneous Soils, *Water Resources Research*, *21*(6), 808-820.

Vernerey, F. J. (2012), The Effective Permeability of Cracks and Interfaces in Porous Media, *Transport in Porous Media*, *93*(3), 815-829.

Wang, K., and G. Huang (2011), Effect of permeability variations on solute transport in highly heterogeneous porous media, *Adv. Water Resour.*, *34*(6), 671-683.

Warrick, A., and D. Myers (1987), Optimization of sampling locations for variogram calculations, *Water Resources Research*, *23*(3), 496-500.

Webster, R., and M. A. Oliver (1993), How large a sample is needed to estimate the regional variogram adequately?, in *Geostatistics Tróia '92: Volume 1*, edited by A. Soares, pp. 155-166, Springer Netherlands, Dordrecht.

Welty, C., and L. W. Gelhar (1994), EVALUATION OF LONGITUDINAL DISPERSIVITY FROM NONUNIFORM FLOW TRACER TESTS, *Journal of Hydrology*, *153*(1-4), 71-102.

Willmann, M., J. Carrera, and X. Sanchez-Vila (2008), Transport upscaling in heterogeneous aquifers: What physical parameters control memory functions?, *Water Resources Research*, *44*(12).

Yoon, H., Q. Kang, and A. J. Valocchi (2015), Lattice Boltzmann-Based Approaches for Pore-Scale Reactive Transport, *Reviews in Mineralogy and Geochemistry*, *80*(1), 393-431.

Zhang, Y.-K., and S. P. Neuman (1990), A quasi-linear theory of non-Fickian and Fickian subsurface dispersion: 2. Application to anisotropic media and the Borden site, *Water Resources Research*, *26*(5), 903-913.

Zhang, Y., M. M. Meerschaert, and R. M. Neupauer (2016), Backward fractional advection dispersion model for contaminant source prediction, *Water Resources Research*, *52*(4), 2462-2473.

Zhao, P., and B. Yu (2006), On model selection consistency of Lasso, *Journal of Machine Learning Research*, *7*(Nov), 2541-2563.

Zinn, B., and C. F. Harvey (2003), When good statistical models of aquifer heterogeneity go bad: A comparison of flow, dispersion, and mass transfer in connected and multivariate Gaussian hydraulic conductivity fields, *Water Resources Research*, *39*(3).

Zinn, B., L. C. Meigs, C. F. Harvey, R. Haggerty, W. J. Peplinski, and C. F. Von Schwerin (2004), Experimental visualization of solute transport and mass transfer processes in two-dimensional conductivity fields with connected regions of high conductivity, *Environ. Sci. Technol.*, *38*(14), 3916-3926.

Zou, H. (2006), The adaptive lasso and its oracle properties, *Journal of the American statistical association*, *101*(476), 1418-1429.

Zou, H., and T. Hastie (2005), Regularization and variable selection via the elastic net, *Journal of the Royal Statistical Society: Series B (Statistical Methodology)*, *67*(2), 301-320.

# SECTION

# 2. CONCLUSIONS

The goal of this study was to model the impact of heterogeneity both in reactive and non-reactive transport using statistical parameters.

Magnesite dissolution was simulated under various hydro geochemical conditions. Overall, permeability ratio had the most significant impact on dissolution rate, porosity and concentration of Mg2+, followed by major direction anisotropy and inlet pH. As the major and minor direction anisotropies decrease, the mineral distribution becomes closer to a homogeneous distribution. Deep learning captured 89% of the variance in the data whereas liner regression only captured 73.2%.

Bromide attenuation time was simulated under various flow rates and transverse dispersivties in heterogeneous porous media. Realization of the porous media were created using statistical parameters such as mean permeability, permeability standard deviation and major and minor direction anisotropy. Overall permeability standard deviation had the most significant impact on the attenuation time, followed by major and minor anisotropy. Lasso regression was used to select the most significant variables and simple linear regression was conducted on the selected variables in an attempt to find the best fitting model. The model then was verified on the test data set which resulted in an $R^2$ score of 0.7083.

It can be concluded that due to the fact that controlling the media's characteristic is very complex in the laboratory, numerical studies have proven to be successful in modeling the solute transport in a vast variety of porous media.

# REFERENCES

Berkowitz, B., Dror, I., Hansen, S.K., Scher, H., 2016. Measurements and models of reactive transport in geological media. Reviews of Geophysics 54, 930-986.

Dentz, M., Gouze, P., Carrera, J., 2011a. Effective non-local reaction kinetics for transport in physically and chemically heterogeneous media. Journal of Contaminant Hydrology 120-21, 222-236.

Dentz, M., Le Borgne, T., Englert, A., Bijeljic, B., 2011b. Mixing, spreading and reaction in heterogeneous media: A brief review. Journal of Contaminant Hydrology 120-21, 1-17.

Espinoza, C., Valocchi, A.J., 1998. TEMPORAL MOMENTS ANALYSIS OF TRANSPORT IN CHEMICALLY HETEROGENEOUS POROUS MEDIA. J. Hydrol. Eng. 3, 276-284.

Gjetvaj, F., Russian, A., Gouze, P., Dentz, M., 2015. Dual control of flow field heterogeneity and immobile porosity on non-Fickian transport in Berea sandstone. Water Resources Research 51, 8273-8293.

Li, L., Peters, C.A., Celia, M.A., 2007. Effects of mineral spatial distribution on reaction rates in porous media. Water Resources Research 43, 17.

Meile, C., Tuncay, K., 2006. Scale dependence of reaction rates in porous media. Adv. Water Resour. 29, 62-71.

Wang, K., Huang, G., 2011. Effect of permeability variations on solute transport in highly heterogeneous porous media. Adv. Water Resour. 34, 671-683.

Yoon, H., Kang, Q., Valocchi, A.J., 2015. Lattice Boltzmann-Based Approaches for Pore-Scale Reactive Transport. Reviews in Mineralogy and Geochemistry 80, 393-431.

# VITA

Mahta Gholizadeh Ansari received a bachelor's degree in Mining Engineering from School of Engineering, University of Tehran in July 2014 and moved to United States of America. In July 2017 she received her M.S. Degree in Geological Engineering from Missouri University of Science and Technology. She worked in Reactive Transport group at Missouri S&T as a Graduate research Assistant. Her research involved reactive transport modeling, aqueous geochemistry, hydrogeology and water rock interactions.